

1

2

3

4

5

6 Cindy Dirscherl^{1,x}, Sara Löchte^{2,x}, Zeynep Hein¹, Janine-Denise Kopicki³, Antonia Regina
7 Harders¹, Noemi Linden¹, Andreas Karner⁹, Johannes Preiner⁹, Julian Weghuber⁴, Maria
8 Garcia-Alai^{5,6}, Charlotte Utrecht^{3,7}, Martin Zacharias⁸, Jacob Piehler^{2,*}, Peter
9 Lanzerstorfer^{4,*}, and Sebastian Springer^{1,*}

10

11

12 ¹Department of Life Sciences and Chemistry, Jacobs University Bremen, Germany;

13 ²Department of Biology and Center for Cellular Nanoanalytics, Osnabrück University, 49076
14 Osnabrück, Germany;

15 ³Heinrich Pette Institute, Leibniz Institute for Experimental Virology, Hamburg, Germany;

16 ⁴University of Applied Sciences Upper Austria, 4600 Wels, Austria;

17 ⁵European Molecular Biology Laboratory, Hamburg Outstation, Hamburg, Germany;

18 ⁶Centre for Structural Systems Biology, Hamburg, Germany;

19 ⁷European XFEL, Schenefeld, Germany;

20 ⁸Physics Department, Technical University of Munich, Garching, Germany;

21 ⁹University of Applied Sciences Upper Austria, 4020 Linz, Austria.

22

23 ^xEqual contribution.

24

25 * To whom correspondence should be addressed:

Sebastian Springer

Department of Life Sciences and
Chemistry
Jacobs University Bremen
Campus Ring 1
28759 Bremen, Germany
s.springer@jacobs-university.de
+49 421 2003243

Peter Lanzerstorfer

School of Engineering
University of Applied Sciences
Austria
Stelzhamerstraße 23
A-4600 Wels, Austria
peter.lanzerstorfer@fh-wels.at
+43 5 080444402

Jacob Piehler

Department of Biology/Chemistry
Osnabrück University
Barbarastr. 11
49076 Osnabrück, Germany
piehler@uos.de
+49 541 969 2800

26

1 **Abstract**

2 At the plasma membrane of mammalian cells, major histocompatibility complex class I
3 molecules (MHC-I) present antigenic peptides to cytotoxic T cells. Following the loss of the
4 peptide and the light chain beta-2 microglobulin ($\beta_2\text{m}$), the resulting free heavy chains
5 (FHCs) can associate into homotypic complexes in the plasma membrane. Here, we investi-
6 gate the stoichiometry and dynamics of MHC-I FHC assemblies by combining a
7 micropattern assay with fluorescence recovery after photobleaching (FRAP) and with single
8 molecule co-tracking. We identify non-covalent MHC-I FHC dimers mediated by the α_3 do-
9 main as the prevalent species at the plasma membrane, leading a moderate decrease in the
10 diffusion coefficient. MHC-I FHC dimers show increased tendency to cluster into higher or-
11 der oligomers as concluded from an increased immobile fraction with higher single molecule
12 co-localization. *In vitro* studies with isolated proteins in conjunction with molecular docking
13 and dynamics simulations suggest that in the complexes, the α_3 domain of one FHC binds to
14 another FHC in a manner similar to the $\beta_2\text{m}$ light chain.

15

1 **Significance Statement**

2 MHC class I molecules are cell surface transmembrane proteins with key functions in
3 adaptive immunity against viral infections. The spatiotemporal organization of fully assem-
4 bled MHC I at the cell surface and its function with respect to trans-interactions with T and
5 NK cells has been studied in detail. By contrast, the consequences of peptide and β_2 m disso-
6 ciation yielding to formation of free heavy chains (FHC) have remained unclear. We have
7 discovered that class I free heavy chains form distinct non-covalent dimers at the cell surface
8 rather than non-specific clustering, and we have identified a dimerization interface mediated
9 by the α_3 domain. We propose that these non-covalent dimers are the basis of distinct signal-
10 ing and endocytic sorting of MHC I FHC. This is to be explored in further work.

11

1 **Introduction**

2 Major histocompatibility class I molecules (MHC-I) fulfil central tasks of the adaptive
3 immune response against infections and malignancies by presenting antigenic peptides to T
4 cells (Comber and Philip, 2014; Kaufman, 2018; Townsend and Bodmer, 1989). MHC-I
5 heterotrimers consist of the polymorphic transmembrane heavy chain (HC), the non-
6 polymorphic soluble light chain beta-2 microglobulin (β_2 m), and the peptide (Townsend et
7 al., 1990, 1989). In addition to this trimer, two more states of MHC-I occur at the cell sur-
8 face, the ‘empty’ HC/ β_2 m heterodimer that lacks peptide (Ljunggren et al., 1990; Sebastián
9 Montealegre et al., 2015), and the monomeric ‘free’ heavy chain (FHC) (Edidin et al., 1997;
10 Geng et al., 2018). Since the binding of peptide and β_2 m is cooperative (Elliott et al., 1991;
11 Gakamsky et al., 1996), HC/ β_2 m heterodimers are conformationally unstable, and loss of
12 peptide leads to the rapid formation of FHCs (schematic in **Figure 1A**) and to the subsequent
13 endocytic removal of FHCs by a sorting mechanism that is not understood (Sebastián Mon-
14 tealegre et al., 2015). For FHCs present at the cell surface, important regulatory functions
15 mediated by homo- and heteromeric interactions in *cis* and *trans* have been proposed (Arosa
16 et al., 2021, 2007; Campbell et al., 2012), which suggest defined spatiotemporal organization
17 and dynamics of FHC in the plasma membrane. Indeed, clustering and covalent dimerization
18 of MHC-I have been identified using a variety of approaches including recombinant proteins
19 and live cells (Allen et al., 1999; Antoniou et al., 2011; Armony et al., 2021; Baia et al.,
20 2016; Blumenthal et al., 2016; Bodnar et al., 2003; Capps et al., 1993; Chakrabarti et al.,
21 1992; Fassett et al., 2001; Ferez et al., 2014; Lu et al., 2012; Makhadiyeva et al., 2012; Matko
22 et al., 1994; Triantafilou et al., 2000); these represent complexes of different and largely un-
23 clear composition, size, and type of intermolecular bonding.

1 Recently, we have achieved direct detection of homomeric FHC interactions in the intact
2 plasma membrane by means of a live-cell two-hybrid micropattern assay (**Figure 1B, C**)
3 (Dirscherl et al., 2018): micrometer-sized patterns of anti-hemagglutinin tag (HA) monoclo-
4 nal antibody are printed onto glass coverslips (Schwarzenbacher et al., 2008; Sevcik et al.,
5 2015). Onto these micropatterns, cells are seeded that express two different MHC-I HC con-
6 structs: one construct has an N-terminal (extracellular) HA tag and thus, while diffusing lat-
7 erally in the plasma membrane, is captured into the printed antibody pattern. The other has no
8 HA tag but a C-terminal (intracellular) green fluorescent protein (GFP) fusion domain (**Fig-**
9 **ure 1B**). Interaction of GFP-tagged HC with micropatterned HA-HC is detected by an in-
10 creased GFP fluorescence of the pattern elements (**Figure 1C**). The system allows the obser-
11 vation of different defined conformational states of class I: with TAP2 (transporter associated
12 with antigen processing)-deficient fibroblasts (which cannot transport peptide into the endo-
13 plasmic reticulum (ER)), empty HC/β₂m heterodimers are present at the cell surface. By add-
14 ing peptide, shifting cells to 25 °C, or incubating at 37 °C, we therefore can accumulate
15 trimers, HC/β₂m heterodimers, or FHCs, respectively, at the cell surface (**Figure 1B** and de-
16 scribed below). These experiments revealed that formation of homomeric MHC-I only takes
17 place in the absence of β₂m, *i.e.*, only between FHCs.

18 We now have uncovered the molecular principles that govern such homomeric MHC-I
19 FHC association in the plasma membrane. Cell micropatterning in conjunction with fluores-
20 cence recovery after photobleaching (FRAP) was used to probe dynamics, stability, and
21 prominence of FHC complexes. We directly demonstrate FHC association in the plasma
22 membrane under physiological conditions by using real-time single-molecule tracking (SMT)
23 and co-tracking (SMCT). Surprisingly, we find that FHCs transiently associate into non-
24 covalent dimers with lifetimes in the sub-second range. Based on our findings that the
25 HC/HC complexes contain no β₂m and that the α₃ domain of the HC is sufficient for dimeri-

1 zation *in vitro* and in cells, we propose a molecular model structure of MHC-I HC/HC dimers
2 supported by *in silico* docking and molecular dynamics (MD) simulation. Our findings clearly
3 differentiate the cell surface dynamics and properties of empty FHCs from the peptide-
4 loaded trimers of MHC-I, pointing to the formation of structurally well-defined HC/HC
5 homodimers that may be responsible for distinct endosomal trafficking and other biological
6 functions previously ascribed to FHCs.

7

8

9 **Results**

10 ***A micropattern assay reveals non-covalent association of MHC class I free heavy*** 11 ***chains***

12 In STF1 cells, which are fibroblasts that cannot load MHC-I with peptides due to a deficiency
13 in the TAP peptide transporter, incubation at 25 °C accumulates murine HC/β₂m heterodimers at the plasma membrane, since at that temperature, dissociation of β₂m and subsequent endocytosis are inhibited (Day et al., 1995; Ljunggren et al., 1990; Sebastián Mon-
14 tealegre et al., 2015). When the temperature is shifted to 37 °C, β₂m dissociates to yield
15 FHCs, and lateral *in cis* interactions between HA-K^b and K^b-GFP (both hybrids of the HC of
16 the murine MHC-I molecule H-2K^b) become visible in the micropattern two-hybrid assay,
17 where the GFP fluorescence arranges in the shapes of the antibody micropattern (**Figure 1C**).
18 When cognate peptide is added to the cells, HC/β₂m/peptide trimers are stable and do not
19 associate with each other (**Figure 2B**) (Dirscherl et al., 2018).

22 Up to six different MHC-I allotypes are present at the cell surface of human and murine
23 cells. To date, though, an interaction of different MHC-I allotypes in the same plasma membrane has not been shown. We therefore tested for such heterotypic interactions between K^b

1 and H-2D^b (D^b). Just as for K^b/K^b, also K^b and D^b FHCs (at 37 °C) interacted with each other,
2 whereas β_2 m-bound heterodimers at 25 °C did not (**Figure 1D**). Hence, our micropattern as-
3 say confirmed that formation of heterotypic FHC interactions is possible.

4 We next asked which molecular characteristics are required for HC/HC interactions, and
5 we first tested whether the HCs are held together by cytosolic disulfide bonds as previously
6 suggested for certain allotypes under oxidizing conditions (Baía et al., 2016; Capps et al.,
7 1993; Makhadiyeva et al., 2012). We replaced the single cysteine in the cytosolic tail of K^b-
8 GFP (residue 332) with a serine and tested for association between this mutant and wild type
9 HA-K^b (**Figure 1E**). K^b(C332S)-GFP and wild type HA-K^b interacted in over 90% of cells,
10 just as the wild type K^b-GFP, demonstrating that cysteine 332 is not required for HC/HC in-
11 teractions.

12 To test more generally for any disulfide bonding in MHC-I interactions, we
13 immunoprecipitated HA-K^b molecules from STF1 cell lysate with an anti-HA antibody. By
14 non-reducing gel electrophoresis, covalent homodimers of K^b were not observed, while the
15 well-described disulfide-linked homodimers of the human MHC-I allotype HLA-B*27:05
16 (Dangoria et al., 2002) were readily detected (**Figure 1F**). We conclude that the K^b FHCs are
17 non-covalently associated and that they do not undergo intramolecular disulfide bonding un-
18 der the conditions of our assay.

19 Since the cysteines in the cytosolic tail of K^b are not required for HC/HC interaction, we
20 hypothesized that FHCs non-covalently associate via their extracellular domains, and that the
21 loss of β_2 m is a prerequisite for HC/HC interaction. As anticipated, a disulfide-stabilized var-
22 iant of K^b-GFP (Y84C/A139C), in which β_2 m dissociation is dramatically decreased (Hein et
23 al., 2014), did not interact with HA-K^b (**Figure 1G**). In agreement with our earlier finding
24 that covalent attachment of β_2 m to the HC also prevents HC/HC association (Dirischerl et al.,

1 2018), this result demonstrates that HC/β₂m heterodimers do not interact with other HC/β₂m
2 heterodimers, nor with FHCs. These findings demonstrate that the MHC class I complexes
3 observed in our system are non-covalent in nature and comprise free heavy chains, devoid of
4 β₂m and peptide.

5

6 ***Free heavy chains associate on TAP-proficient cells***

7 So far, we used TAP2-deficient STF1 cells to obtain homogeneous populations of free
8 heavy chains at the cell surface. Since MHC-I HC/β₂m heterodimers and FHCs both exist at
9 the cell surface of wild type cells (Day et al., 1995; Ljunggren et al., 1990; Ortiz-Navarrete
10 and Hammerling, 1991, p.), we next tested whether FHCs also associate in cells with wild
11 type TAP function (schematic in **Figure 2A**). Following the 25 °C to 37 °C temperature shift
12 that triggers FHC formation, we performed the same anti-HA antibody two-hybrid
13 micropatterning assay with HA-K^b and K^b-GFP as above (in **Figure 1B and C**). Again, the
14 punctate GFP fluorescence signifies the recruitment of K^b-GFP fusion to the printed patterns
15 of the anti-HA antibodies, mediated by the HA-K^b fusion. We quantified K^b HC/HC interac-
16 tion over time in STF1/TAP2 cells, which are able to load class I molecules with peptides, by
17 GFP fluorescence contrast analysis between pattern elements and interspaces. Interactions
18 increased in TAP2-positive and in TAP2-deficient cells with the same dynamics and reached
19 a maximum after ca. 60 min of incubation at 37 °C (**Figure 2B, C**), with the kinetics likely
20 governed by the dissociation of β₂m from the HC/β₂m heterodimers, which occurs on this
21 timescale (Sebastián Montealegre et al., 2015). As expected, HC/β₂m/peptide trimers, stabi-
22 lized by cognate SIINFEKL peptide, did not show any interaction (**Figure 2B**). This experi-
23 ment confirms that HC/HC interactions indeed take place at the surface of TAP2-proficient
24 cells. In addition, these experiments again confirm our earlier observations (Dirscherl et al.,

1 2018) that the HC/HC interaction occurs only between FHCs: when dissociation of β_2 m is
2 inhibited by low temperature (**Figure 1 DEG**) or by added peptide (**Figure 2 BD**), the inter-
3 action does not occur. The same experiments also strongly suggest that the recruitment of the
4 K^b -GFP fusion to the pattern elements specifically reports on the interaction between MHC
5 class I molecules (since it depends on their conformation) and is not due to an attraction be-
6 tween K^b -GFP and other surface proteins, e.g., adhesion molecules, that might have been
7 attracted to the plasma membrane above the pattern elements.

8

9 ***FHC association slows down cell surface diffusion of MHC-I***

10 Since dimers and oligomers of FHCs have more transmembrane domains (TMDs) than
11 single HC/ β_2 m/peptide complexes, we hypothesized that they should diffuse more slowly in
12 the plasma membrane (Gambin et al., 2006; Wilmes et al., 2015a). We therefore carried out
13 total internal reflection fluorescence (TIRF) fluorescence recovery after photobleaching
14 (FRAP) experiments on STF1 cells with HA- K^b and K^b -GFP on surfaces with or without
15 micropatterns (**Figure 2D**) and quantified the recovery dynamics (**Figure 2E**). Diffusion
16 constants of FHCs (– peptide) were significantly decreased as compared to HC/ β_2 m/peptide
17 complexes (+ peptide; **Figure 2F**), suggesting that FHCs form complexes. The moderate de-
18 crease of $\approx 40\%$ is in line with the formation of dimers rather than clustering into larger com-
19 plexes. Since this effect occurred both in cells seeded on the pattern elements (on pattern) and
20 in cells seeded off the micropatterns (off pattern), we conclude that the micropatterns are not
21 required for HC/HC interactions, i.e., that the interactions are not an artefact of the two-
22 hybrid micropattern assay. This **statement** is also supported by the co-immunoprecipitation of
23 MHC-I molecules in the absence of micropatterns (Dirischerl et al., 2018; Triantafilou et al.,
24 2000). Diffusion constants of HC/ β_2 m/peptide trimers on pattern and off pattern were not

1 significantly different, which demonstrates that the antibody micropatterns themselves do not
2 impede the diffusion of plasma membrane proteins.

3 In the FRAP experiments, a portion of K^b -GFP appeared immobile on a timescale of sec-
4 onds as evidenced by the incomplete fluorescence recovery (**Fig. 2E**). This immobile fraction
5 is significantly higher for FHCs than for HC/ β_2 m/peptide trimers (**Fig. 2G**). This observation
6 is readily explained for K^b -GFP bound to HA- K^b molecules immobilized within
7 micropatterns, but it is remarkable for the FHCs on cells outside of the micropattern (gray
8 column in **Fig. 2G**). There, it may be ascribed to the formation of large oligomers, and/or to
9 the association of FHCs with immobile structures, such as the cytoskeleton and/or due to se-
10 questration in endocytic membrane compartments (Bondar et al., 2020; Ibach et al., 2015;
11 Mylvaganam et al., 2018; Vámosi et al., 2019). From the FRAP curves, the exchange rate of
12 the freely diffusing pool of K^b -GFP into and out of the bleached regions of interest (ROIs) is
13 obtained through a bi-exponential fit as the slow recovery rate (k_{slow}) (**Figure 2H**, solid bars);
14 the fast recovery rate k_{fast} represents free diffusion (Sprague and Mcnally, 2005)(see the Ma-
15 terials and Methods). On the pattern elements, the k_{slow} of FHCs was much smaller than in
16 cells outside the patterns, suggesting a half-time of dissociation from the pattern-bound im-
17 mobile associations of about 140 seconds. Likewise, the fluorescence signal of pattern ele-
18 ments in the immediate vicinity of the bleached region remained unaltered, indicating that no
19 detectable exchange of K^b -GFP between the enriched HA- K^b regions occurs on the second
20 timescale (**Figure 2S3**). This very slow exchange of K^b -GFP molecules associated on pattern
21 elements suggests either multiple association and dissociation events in a small radius due to
22 densely immobilized binding partners, or a very stable association of the immobile FHCs (see
23 the discussion). Taken together, the data from **Figure 2** show reduced diffusion rates of K^b

1 FHCs at the cell surface compared to HC/β₂m/peptide complexes, which is most easily ex-
2 plained by homotypic association of the former.

3

4 ***Transient FHC dimerization directly observed at single molecule level***

5 We therefore turned to directly visualizing FHC diffusion and interaction in the plasma
6 membrane under physiological conditions by single molecule tracking (SMT) and co-
7 tracking (SMCT) (Moraga et al., 2015; Sevcik et al., 2015; Wilmes et al., 2020a). STF-1
8 cells transiently expressing K^b with its N-terminus fused to monomeric GFP (GFP-K^b) were
9 imaged by TIRF microscopy. The GFP tag was labeled with photostable fluorescent dyes by
10 using equal concentrations of anti-GFP nanobodies conjugated to either ATTO Rho11
11 (^{Rho11}NB) or ATTO 643 (^{ATTO643}NB), with one nanobody binding one GFP molecule, ensur-
12 ing selective imaging of K^b in the plasma membrane and tracking with high fidelity (**Fig-**
13 **ure 3A**). Imaging was performed at 37 °C to induce formation of FHC in the absence of the
14 peptide, while replenishment of GFP-K^b/β₂m dimers from the ER was inhibited by Brefeldin
15 A (BFA).

16 After labeling with ^{Rho11}NB and ^{ATTO643}NB, individual K^b subunits were observed at densi-
17 ties of <1 molecule/μm² diffusing randomly in the plasma membrane (**Supplementary Mov-**
18 **ie S1, Supplementary Figure S3A**). Co-tracking analysis revealed homomeric interaction of
19 K^b FHCs in the absence of peptide, whereas these events were very rare for peptide-loaded
20 K^b (**Figure 3B-D**). As a positive control for the formation of homodimers, a crosslinker
21 based on the tandem anti-GFP nanobody LaG16 (Fridy et al., 2014), which recognizes a dif-
22 ferent epitope than the labeled nanobodies, was added to the medium. While dimerizing of K^b
23 via the GFP tag resulted in a nominal fraction of ≈38% (median) co-locomoting molecules,
24 only ≈3% of the FHCs were found associated, indicating weak interaction of FHCs at these

1 low cell surface expression levels of K^b (\approx 1 molecule/ μm^2 in total, corresponding to <5000
2 molecules/cell).

3 From the trajectory analysis, we determined the diffusion coefficients of individual MHC-
4 I molecules by mean square displacement analysis (**Figure 3E, Supplementary Figure**
5 **S3B**). In the absence of peptide, diffusion of FHCs was significantly slower than in the pres-
6 ence of the peptide. This decrease in single molecule diffusion coefficients supports interac-
7 tion of FHCs in the plasma membrane. A similar decrease in the diffusion coefficient was
8 observed upon dimerization of peptide-loaded K^b with the tandem nanobody, suggesting that
9 FHCs associate into dimers. Indeed, largely identical diffusion coefficients were found for
10 the fraction of molecules identified as dimers by SMCT (**Supplementary Figure S3C, Ta-**
11 **ble 1**). Strikingly, the diffusion constants obtained by SMT for peptide-loaded K^b and for
12 FHC from SMT are consistent with those obtained by FRAP experiments under the same
13 conditions (**Figure 2E, Table 1**), highlighting that similar phenomena are being probed by
14 these complementary techniques. Tracking analysis revealed a slightly elevated immobile
15 fraction of $\sim 20\%$ for K^b in the absence of the peptide compared to $\approx 17\%$ for peptide-loaded
16 K^b (**Figure 3F**). Again, a similar effect was observed for artificially dimerized, peptide-
17 loaded K^b, corroborating the dimeric stoichiometry of associated FHCs. Importantly, the
18 “immobile fraction” in SMT refers to much shorter time and length scales as compared to
19 FRAP (cf. methods section), and therefore, the absolute numbers are not comparable. Within
20 the immobile fraction, a higher level of FHC was found associated, as compared to the mo-
21 bile fraction (**Figure 3G**). Overall, the single molecule diffusion analyses suggest that FHC
22 dimers have an increased propensity to be immobilized at the plasma membrane, probably by
23 clustering that may be related to endocytosis. Interestingly, this feature is reproduced by arti-
24 ficial dimerization of intact MHC-I by a crosslinker, suggesting that FHC dimerization is a
25 switch regulating its cell surface dynamics.

1 SMCT analysis moreover revealed dissociation of FHC homomers, confirming its transi-
2 ent nature (**Figure 3B**, **Supplementary Movies S2-5**). We estimated the lifetime of FHC
3 complexes from co-trajectory length histograms. Fitting of an exponential decay revealed a
4 significantly shorter lifetime for FHC co-trajectories compared to the average co-tracking
5 lifetime determined for stably NB-crosslinked K^b, which is limited by co-tracking fidelity and
6 photobleaching (**Figure 3H**). Taken together, the SMT and SMCT results of **Figure 3** direct-
7 ly confirm a transient homotypic HC/HC interaction in the plasma membrane that leads to
8 reduced diffusion velocity and immobilization, in line with the FRAP experiments. Since the
9 degree of association was low, and higher-order oligomerization was not observed, we pro-
10 pose that HC/HC interactions are weak and have dimeric stoichiometry.

11

12 ***The α_3 domain of K^b forms dimers and is sufficient for FHC association***

13 We next explored the molecular mechanism of HC/HC interaction. Since cytosolic
14 cysteines are not involved (**Figure 1E, F**) and dissociation of β_2 m is necessary (**Figure 1G**),
15 we hypothesized that HC/HC interactions involve the extracellular portion of the HCs. To
16 determine more precisely which domains are involved, we used STF1 cells in the
17 micropattern assay that expressed constructs of K^b that lacked the α_1/α_2 domain. Remarka-
18 bly, α_3 -GFP showed excellent copatterning with HA-K^b-RFP (fused to red fluorescent pro-
19 tein; **Figure 4A**) and with HA- α_3 (**Figure 4B**), demonstrating that isolated α_3 domains can
20 bind to each other on the surface of live cells. Indeed, the isolated, soluble α_3 domain of K^b,
21 when refolded *in vitro*, showed (after testing of its folded state by fluorescence spectroscopy,
22 **Supplementary Figure S4C**) significant formation of homodimers in size exclusion chroma-
23 tography (SEC; **Figure 4C**), while no prominent higher-order complexes were observed.
24 These α_3 homodimers were not linked by disulfide bonds as shown by nonreducing gel elec-

1 trophoresis (**Figure 4D**), just like the interaction of full-length FHC in the plasma membrane
2 (**Figure 1F**). Given the 1:1 peak ratio observed at 10 μ M protein concentration, a binding
3 affinity of 10 to 20 μ M can be estimated for this interaction. The non-covalent α_3
4 homodimers were also detectable by native mass spectrometry (MS) in a concentration-
5 dependent manner, and they easily separated into the monomers when the collision cell volt-
6 age was increased in an MS/MS experiment, suggesting a low-affinity interaction (**Fig-**
7 **ure 4E-G, Supplementary Figure S4A**). These biochemical results, together with the obser-
8 vations on the α_3 constructs above, suggest that FHC dimerization in the plasma membrane is
9 at least partly based on the intrinsic affinity between the α_3 domains. To investigate whether
10 the α_3 domain is indeed required for FHC dimerization, we performed a co-patterning exper-
11 iment with an HA-K^b fusion protein that lacked the α_3 domain (HA-K^b($\Delta\alpha_3$)-RFP) and K^b-
12 GFP and found the interaction significantly reduced, but still measurable (**Supplementary**
13 **Figure S4B**), which suggests that the α_1/α_2 domain is also involved in the interaction.
14

15 *A molecular model of the K^b HC dimer*

16 To image a possible arrangement of the K^b heavy chains in a dimer, we used molecular
17 docking. A starting geometry was obtained by placing the α_3 domain of one K^b HC in the
18 same position as the β_2 m in the original K^b HC/ β_2 m heterodimer and adjusting the α_1/α_2
19 superdomain to avoid sterical overlap. The structure was then energy-minimized and further
20 refined by Molecular Dynamics (MD) simulations (**Figure 5A**). During MD simulations of
21 400 ns, no signs of dissociation were observed, and a stable root-mean-square deviation
22 (RMSD) from the start structure was reached (**Supplementary Figure S5**). In the model, the
23 α_3 domain of one FHC substitutes for β_2 m, binding both the α_3 domain and the α_1/α_2
24 superdomain of another FHC with a buried interface area (BSA) of 2480 \AA^2 , which is compa-

1 rable to the BSA of 2740 Å² between β₂m and the HC in heterodimers (**Figure 5B**, bottom),
2 and to other stable protein complexes (Bahadur and Zacharias, 2008). Similar results were
3 obtained with other arrangements of the two heavy chains (not shown).

4

5 Discussion

6 Interactions of MHC-I FHC with FHC of the same allotype, of different allotypes, and
7 even with other cell surface proteins have been proposed to play an important role in regulat-
8 ing adaptive and innate immune responses (Arosa et al., 2021, 2007; Campbell et al., 2012),
9 but the molecular principles **that govern** FHC interactions have remained unclear. By com-
10 bining live cell interaction and diffusion analysis using cell micropatterning and FRAP as
11 well as SMT and SMCT, we have shown here that, after losing β₂m, murine H-2K^b MHC-I
12 molecules at the cell surface interact in a homotypic and heterotypic manner to form dimers,
13 which are transient with a stability on the second timescale. **The α₃ domains of the FHCs**
14 **alone are sufficient for such interactions, but it is conceivable that the α₁/α₂ domain is also**
15 **involved: in addition to the α₃-α₃ interaction, the α₃ domain might also bind to the α₁/α₂ do-**
16 **main of the other protein, or the α₁/α₂ domains of the two proteins might interact with each**
17 **other. We cannot currently distinguish these possibilities.**

18 While we observed a somewhat increased tendency of FHCs to form higher oligomers, our
19 data surprisingly identify non-covalent FHC dimers as the prevalent species at the cell sur-
20 face. We analyzed the diffusion properties of FHCs and HC/β₂m/peptide trimers at different
21 cell surface expression levels by FRAP and SMT. FRAP experiments were carried out at high
22 surface densities, which probably exceeded the typical endogenous cell surface expression
23 levels of 10⁵ copies/cell (Spack and Edidin, 1986). By contrast, SMT was performed at densi-
24 ties of ≈1 molecule/μm², *i.e.*, <5000 molecules/cell. Despite these differences in expression

1 levels, we found highly consistent diffusion coefficients D by both FRAP and SMT, which
2 revealed moderately decreased mobility upon dissociation of β_2 m (**Table 1**). However, under
3 both conditions, the decrease in D was \approx 40–50%, which perfectly agrees with the change in D
4 upon dimerizing intact MHC-I by the tandem nanobody (**Figure 3E**). Likewise, we and oth-
5 ers have previously observed very similar decreases of 30–50% upon dimerization of cell
6 surface receptors (Ho et al., 2017; Low-Nam et al., 2011; Moraga et al., 2015; Richter et al.,
7 2017; Váradi et al., 2019; Wilmes et al., 2015a, 2020a), corroborating that the mobile HC/HC
8 complexes are mostly dimers.

9 Direct detection of FHC interaction by SMCT corroborated transient, non-covalent dimer-
10 ization and only minor clustering into higher oligomers. Estimated lifetime of the non-
11 covalent FHC/FHC dimer ($t_{1/2} = 220 \pm 150$ ms, **Figure 3G, H**) were well within the measura-
12 ble range, *i.e.*, substantially below the apparent half-life obtained for the quasi-irreversibly,
13 nanobody-crosslinked control ($t_{1/2} > 10$ s), which defined the limit of co-tracking fidelity. To-
14 gether with the immunoprecipitation experiments (**Figure 1F**) and micropatterning of FHC
15 lacking free cysteines (**Figure 1E**), these observations clearly establish that the FHC mole-
16 cules at the plasma membrane are not covalently linked. The short half-life and the non-
17 covalent monomer-dimer equilibrium observed by size exclusion chromatography at higher
18 micromolar concentration for the isolated α_3 domain (**Figure 4CD**), as well as the mass spec-
19 trometry data (**Figure 4E-G**), point to a low-affinity interaction with a dimerization K_d of
20 perhaps 10 to 20 μ M. Previous quantitative studies on affinity-dimerization correlation of
21 heterodimeric cytokine receptors (Wilmes et al., 2015a) would predict efficient FHC dimeri-
22 zation at physiological densities above 10 molecules/ μ m 2 , which is in line with the endoge-
23 nous MHC-I expression level. The relatively low level of dimerization we observed by
24 SMCT can be rationalized with the high background of endogenous MHC-I that are unla-

1 beled and invisible to us. In line with this observation, the decrease of the diffusion coeffi-
2 cient in SMT was much more prominent than the dimer fraction identified by SMCT. This
3 interpretation is in line with the observation that more efficient interaction was observed at
4 the elevated cell surface expression levels used in micropatterning experiments.

5 The weak and transient nature of HC/HC dimerization seen by SMT is similar to the na-
6 ture of cell surface protein-protein association measured in other systems (Lin et al., 2014). It
7 does not conflict with the clear and stringent patterning of the GFP fusion in the
8 micropattern/FRAP experiments. In the latter, the concentration of HA-tagged bait HCs is
9 considerably higher due to their immobilization by the antibodies, which prevents their endo-
10 cytosis, and this probably creates an affinity matrix for the GFP fusions that can retain them
11 for many seconds due to rebinding events. This also suggests that in endosomes, whose inter-
12 nal volume is very small, HC/HC interaction might be potentiated due to the increase in the
13 concentration of the monomers compared to the plasma membrane.

14 In line with the observation of non-covalent dimerization in the plasma membrane, we ob-
15 tained a robust structural model of a self-contained K^b FHC homodimer. The atomistic model
16 (**Figure 5**) was derived from the experimental findings that dissociation of β_2m is required,
17 that the α_3 domains are sufficient, and that a direct α_3/α_3 interaction exists (**Figures 1E, 4A-**
18 **C**). We propose that β_2m dissociation exposes a binding site on the FHC for the α_3 domain of
19 another FHC. However, other arrangements of the two FHCs in a dimer are theoretically pos-
20 sible, and only experimental data will give a definitive answer.

21 Several findings in the literature are consistent with the formation of complexes of MHC
22 class I HCs in the absence of β_2m and peptide; this applies both to the 'classical', or class Ia,
23 proteins HLA-A/B/C (and in mouse: H-2D/K/L) as well as to the 'non-classical', or class Ib,
24 protein HLA-F (Armony et al., 2021; Bodnar et al., 2003; Chakrabarti et al., 1992; Matko et

1 al., 1994; Triantafilou et al., 2000). Still, it is important to differentiate these HC/HC dimers
2 from class I associations described elsewhere (partially reviewed in (Arosa et al., 2021, 2007;
3 Campbell et al., 2012)), namely homo- and heterotypic HC/β₂m/peptide trimers that are cova-
4 lently dimerized via disulfide bonds in their cytosolic tails (Capps et al., 1993; Makhadiyeva
5 et al., 2012) and that may play a role in binding the LILRB NK cell receptor (Baia et al.,
6 2016); the non-covalent nano- and microscale clusters of HC/β₂m/peptide trimers (not de-
7 tected in our system) that may stem from the fusion of exocytic vesicles with the plasma
8 membrane and that may play a role in TCR recognition (Blumenthal et al., 2016; Ferez et al.,
9 2014; Fooksman et al., 2006; Lu et al., 2012); the macroscopic ‘clusters’ of class I molecules
10 at the signaling interface between cells (Fassett et al., 2001) and the covalent dimers of the
11 HLA- B*27:05 heavy chain that are linked by disulfide bonds through Cys-67 (Chen et al.,
12 2017), though our non-covalent HC/HC dimers may be a precursor to the formation of the
13 latter.

14 The unexpected discovery that FHCs non-covalently associate into defined dimers allows
15 exciting hypotheses of their distinct functional properties. FHC dimers might be responsible
16 for the immunomodulatory functions of cell surface heavy chains, *i.e.*, the stabilization of
17 MHC-I trimers to assist T cell activation (Geng et al., 2018; Schell, 2002) and direct binding
18 of FHCs to receptors on other cells (for example, FHCs of HLA-F binding to activating re-
19 ceptors on NK cells (Dulberger et al., 2017, 2017; Goodridge et al., 2013)). Furthermore,
20 dimerization of FHCs might enhance endocytosis in order to remove the non-functional
21 FHCs, which themselves cannot activate T cells and are known to be short-lived
22 (Mahmutefendic et al., 2011; S. Montealegre et al., 2015); alternatively or additionally, such
23 associated HCs may bind to other proteins *in cis* and promote their removal from the plasma
24 membrane. Such endocytic removal might be achieved by altered endosomal routing, since

1 the local density of membrane proteins in endosomes is higher than at the plasma membrane,
2 and thus, efficient dimerization of MHC-I FHCs is expected. In such a scenario, even transi-
3 ent oligomerization in endosomes might prevent the return of internalized MHC-I FHCs to
4 the cell surface (S. Montealegre et al., 2015). Taken together, the presence of non-covalent,
5 transient FHC dimers points to exciting new aspects in the regulation of MHC-I functions
6 with much potential for further investigation.

1 **Materials and Methods**

2 **Cells and cell lines**

3 TAP-deficient human STF1 fibroblasts (kindly provided by Henri de la Salle,
4 Etablissement de Transfusion Sanguine de Strasbourg, Strasbourg, France) were cultivated at
5 37 °C and 5% CO₂ in Earle's minimum Essential Medium (MEM) with stable glutamine
6 supplemented with 10% fetal bovine serum (FBS), non-essential amino acids and HEPES
7 buffer without addition of antibiotics.

8

9 **Genes, vectors, and gene expression**

10 HA-K^b and K^b-GFP constructs were described previously (Dirscherl et al., 2018). HA-K^b
11 carries an influenza hemagglutinin (HA) tag at the N terminus of the full-length murine H-
12 2K^b, whereas K^b-GFP carries a GFP domain at the C terminus of H-2K^b. The D^b-GFP
13 construct is analogous to the K^b-GFP construct. The α_3 -GFP construct consists of the H-2K^b
14 signal sequence and residues 204-369 of H-2K^b, including transmembrane and cytosolic
15 domains. The HA-K^b($\Delta\alpha_3$)-RFP construct, compared to HA-K^b, lacks residues 204-294 and
16 carries an additional RFP (red fluorescent protein) taken from pcDNA3-mRFP (see the key
17 resources table). The GFP-K^b construct used in single-molecule imaging consists of a signal
18 sequence and GFP fused to the N terminus of H-2K^b itself lacking a signal sequence. Amino
19 acid numbering of K^b in this paragraph includes the signal sequence.

20 Stable cell lines were generated by lentiviral transduction as described (Hein et al., 2014),
21 and transient transfection was achieved by electroporation (Garstka et al., 2007) or by calci-
22 um phosphate precipitation (Graham and van der Eb, 1973) as described.

23

1 **Micropattern assay**

2 **Photolithography.** Silicon master molds were prepared by semiconductor photolithography as described previously (Dirscherl et al., 2017).

4 **PDMS stamps and Antibody Patterns.** PDMS stamps were generated from basic elastomer and curing agent (Sylgard 184 Silicone Elastomer Kit) as described previously (Dirscherl et al., 2017).

7 **Patterning cell surface proteins.** Coverslips with antibody pattern were placed into sterile 6-well plates. Cells were immediately seeded as indicated at a concentration of ca. 50 000 9 cells per well. Usually, cells were incubated for 4-6 hours at 37 °C for adhesion and then 10 shifted to 25 °C to accumulate MHC-I molecules at the cell surface. Samples were then kept 11 at 25 °C to increase cell surface heterodimer levels or shifted back to 37 °C for 3-4 hours to 12 induce FHCs by dissociation of β_2 m.

13 **Dyes.** Purified antibodies were labeled with Alexa Fluor 647 NHS ester (Thermo Fisher 14 Scientific, Darmstadt, Germany) according to the manufacturer's protocol.

15 **Peptides.** The K^b-specific peptide SL8 (SIINFEKL in the single-letter amino acid code) 16 was synthesized by GeneCust (Ellange, Luxemburg) and emc microcollections (Tübingen, 17 Germany) and purified by HPLC (90% purity). Peptides were added to the cells at a final 18 concentration of 2 μ M for 15-30 min at 37 °C to induce peptide binding (Dirscherl et al., 19 2018).

20 **Washing and fixation.** Cells were washed with phosphate buffered saline (PBS), 10 mM 21 phosphate pH 7.5, 150 mM NaCl), fixed with 3% paraformaldehyde (PFA), and observed by 22 confocal laser scanning microscopy (cLSM).

23 **Microscopy.** We used a confocal laser scanning microscope (LSM 510 Meta, Carl Zeiss 24 Jena GmbH, Germany) equipped with argon and helium-neon lasers at 488, 543, and 633 nm.

1 Images were recorded with a 63× Plan Apochromat oil objective (numerical aperture 1.4) at a
2 resolution of 1596 × 1596 pixels. Data acquisition was performed with the LSM 510 META
3 software, release 3.2 (Carl Zeiss Jena). During image acquisition, patterns and cells were im-
4 aged in the same focal plane at a pinhole of 1 Airy unit. Image analysis and processing were
5 performed using ImageJ (National Institutes of Health, Bethesda, USA). Image processing
6 comprised cropping, rotation and adjustment of brightness and contrast levels. Experiments
7 in Figure 1 were repeated at least three times each.

8

9 **Recombinant \square_3 domain of H-2K^b**

10 The \square_3 domain of H-2K^b (residues 205-295) was cloned into pET3a (preceded by the resi-
11 dues MAIQR and followed by DRDM) and expressed in *E. coli* BL21(DE3) *pLysS*, refolded
12 *in vitro* as described, and isolated by size exclusion chromatography (SEC) on a Cytiva
13 Hiload Superdex 200 16/600 column (Anjanappa et al., 2020). Molecular weights of the
14 peaks were determined by comparison to SEC protein standards (Cytiva), namely bovine
15 thyroglobulin (670 kDa), bovine gamma globulin (158 kDa), chicken ovalbumin (44 kDa),
16 horse myoglobin (17 kDa), and vitamin B12 (1.35 kDa). The D5 fraction, corresponding to
17 the elution peak at approximately 20-30 kDa, was boiled with or without DTT (0.6 M final
18 concentration) in sample buffer (LSB) (350 mM Tris-Cl pH 6.8, 10.28% sodium dodecyl
19 sulfate (SDS), 36% glycerol 0.012% bromophenol blue). Inclusion body extract boiled with-
20 out DTT (non-reducing) served as positive control for the formation of covalent oligomers.
21 Protein quality control after refolding and SEC was performed by nanoscale differential
22 scanning fluorimetry (nanoDSF) runs (see **Figure 4S2**) acquired with a Nanotemper Prom-
23 theus NT.48 fluorimeter (Nanotemper, Munich) controlled by PR.ThermControl (version
24 2.1.2).

1

2 **Precipitation of surface class I**

3 TAP2-deficient STF1 cells expressing either CE3-HA-K^b or CE3-HA-B*27:05 were kept
4 overnight at 25 °C and then pretreated with tris(2-carboxyethyl)phosphine (TCEP; 1 mM,
5 10 min), labeled with 400 nm of Bio-MPAA-K3 (5 min) at room temperature (RT) (Rein-
6 hardt et al., 2014). Lysis was performed in native lysis buffer (50 mM Tris Cl (pH7.4),
7 150 mM NaCl, 5 mM EDTA, and 1% Triton X100) for 1 hour at 4 °C. Biotinylated surface
8 proteins were then isolated with neutravidin-coated agarose beads (Thermo Fisher Scientific,
9 Darmstadt Germany). The isolates were boiled at 95 °C for 7 min in the presence (reducing)
10 or absence (non-reducing) of 10 mM dithiothreitol (DTT) in sample buffer as described
11 above. Samples were separated by SDS-PAGE and transferred onto polyvinylidene fluoride
12 (PVDF) membranes. MHC molecules were visualized on the membranes with polyclonal
13 rabbit anti-HA antibody as primary antibody (ab9110, Abcam, Cambridge, United Kingdom)
14 and alkaline phosphatase-conjugated anti-rabbit serum from goat as secondary antibody
15 (1706518, Biorad, Munich, Germany). The signals were visualized by treating the blot with
16 BCIP/NBT substrate (B1911, Sigma Aldrich, St. Louis, Missouri, United States).

17

18 **Flow cytometry**

19 For verification of cell surface levels of MHC-I, flow cytometry was performed with anti-
20 HLA class I antibody W6/32 (Barnstable, 1978) and anti-HA antibody (12CA5, described in
21 key resources table). Antibody-antigen complexes were labeled with goat secondary antibody
22 against mouse IgG conjugated with allophycocyanin (APC) (115-135-164, Dianova, Ham-
23 burg, Germany). Fluorescent signal was recorded by a CyFlow1Space flow cytometer
24 (Sysmex- Partec, Norderstedt, Germany) and analyzed by Flowjo, LLC software.

1

2 **FRAP**

3 **Microcontact printing and antibody patterning for total internal reflection fluores-**
4 **cence (TIRF) microscopy** was performed as described previously (Lanzerstorfer et al.,
5 2020). In short, a field of a large-area PFPE elastomeric stamp (1 μ M grid size), obtained by
6 the EV-Group (St. Florian am Inn, Upper Austria, Austria), was cut out, and washed by
7 flushing with ethanol (100%) and distilled water. After drying with nitrogen, the stamp was
8 incubated in 50 mL bovine serum albumin (BSA) solution (1 mg/mL) for 30 min. This step
9 was followed by washing the stamp again with PBS and distilled water. After drying with
10 nitrogen, the stamp was placed with homogeneous pressure onto the clean epoxy-coated glass
11 bottom of a 96-well plate and incubated overnight at 4 °C. The next day, the stamp was
12 stripped from the glass with forceps, and the glass bottom was bonded to a 96-well plastic
13 casting with adhesive tape (3M) and closed with an appropriate lid. For the live cell experi-
14 ments, a reaction chamber was incubated with 100 μ L streptavidin solution (50 μ g/mL) and
15 incubated for 30 min at room temperature. After washing two times with PBS, 100 μ L
16 biotinylated antibody solution (10 μ g/mL) was added for 30 min at room temperature **result-**
17 **ing in an antibody surface coverage of > 85% (Supplementary Figure S1AB)**. Finally, the
18 incubation wells were washed twice with PBS, and cells were seeded at defined cell density
19 for the live cell microscopy analysis. The cells were allowed to attach to the surface for at
20 least 3-4 h prior to imaging to ensure a homogeneous cell membrane/substrate interface,
21 which is a prerequisite for quantitative TIRF microscopy. **Deformation of the plasma mem-**
22 **brane on top of the pattern elements was excluded, since control cells that were stained with**
23 **the lipophilic tracer DiD (1,1'-dioctadecyl-3,3,3',3'-tetramethylindodicarbocyanine), which**
24 **stains the plasma membrane uniformly, showed no patterning (Supplementary Figure S1C)**.

1 For negative control to test the adhesion of the antibodies, anti-HA antibody (Abcam,
2 ab26228) was labeled with a Zenon Alexa Fluor 488 IgG Labeling Kit (Thermofisher,
3 Z25102), printed, bleached, and fluorescence recovery was quantified as described below
4 (**Supplementary Figure S2AB**). In a second control experiment, binding and dissociation of
5 a construct with both tags (HA-K^b-GFP) from the antibody micropattern was tested, which
6 only accounted for less than 20% of the mobility of the K^b fraction (**Supplementary Figure**
7 **S2C**). Dissociation of Kb-GFP from micropattern elements was negligible (**Supplementary**
8 **Figure S2DE**). Thus, in our experiments, k_{slow} was determined by the binding events between
9 K^b-GFP and other K^b molecules.

10

11 **Live-cell TIRF microscopy.** The detection system was set up on an epi-fluorescence mi-
12 croscope (Nikon Eclipse Ti2). A multi-laser engine (Toptica Photonics, Munich, Germany)
13 was used for selective fluorescence excitation of GFP at 488 nm and RFP at 568 nm. The
14 samples were illuminated in total internal reflection (TIR) configuration (Nikon Ti-LAPP)
15 using a 60x oil immersion objective (NA = 1.49, APON 60XO TIRF). After appropriate fil-
16 tering with standard filter sets, the fluorescence was imaged onto a sCMOS camera (Zyla 4.2,
17 Andor, Northern Ireland). The samples were mounted on an x-y-stage (CMR-STG-MHIX2-
18 motorized table, Märzhäuser, Germany), and scanning of the larger areas was supported by a
19 laser-guided automated Perfect Focus System (Nikon PFS).

20 **TIR-FRAP experiments and calculation of diffusion coefficients.** FRAP experiments
21 were carried out on an epi-fluorescence microscope as described above. Single patterns (or
22 equivalent ROIs with 1 μ M in diameter in unpatterned cells) were photobleached (Andor
23 FRAPPA) with a high-intensity laser pulse (488 nm) applied for 500 ms. Recovery images
24 were recorded at indicated time intervals. Normalization of data was done by pre-bleach im-

1 ages, and first data analysis was carried out using NIS Elements software package (Nikon).
2 Further data processing was done in Graphpad Prism. Resulting FRAP curves were plotted
3 based on the standard error of the mean and fitted using a bi-exponential equation. Kinetic
4 FRAP parameters were directly obtained from curve fitting with the following model as-
5 sumptions: Since unhindered MHC-I diffusion (e.g., off pattern and/or after peptide treat-
6 ment; Fig. 2E) was found to be much faster than the recovery within our pattern elements, we
7 applied a diffusion-uncoupled recovery scheme (Sprague and McNally, 2005). Here, after the
8 photobleaching step, fluorescent molecules rapidly diffuse throughout the bleached
9 micropattern, and only bound bleached molecules remain inside the spot. The bleached mole-
10 cules then gradually dissociate from their binding sites. Unbleached molecules can then re-
11 place the bleached molecules at the binding sites as they become vacant. The diffusion-
12 uncoupled FRAP recovery curve consists of two separable components: the early recovery
13 due to diffusion and the slower recovery due to exchange at binding sites, and can be fitted
14 using a diffusion-uncoupled two-component fit:

$$15 \quad Y = Y_{t=0} + A_1(1 - e^{-k_{fast} \cdot x}) + A_2(1 - e^{-k_{slow} \cdot x}),$$

16 where A_1 is the amplitude of the fast-diffusing population, A_2 the amplitude of the slow
17 diffusing population (binding reaction), and k_{fast} and k_{slow} are the rate constants of A_1 and A_2 ,
18 respectively.

19 Diffusion coefficients were obtained using the initial image recordings and the simFRAP
20 plugin for ImageJ (Blumenthal *et al.*, 2015).

21 **Temperature-induced K^b associations.** Temperature-dependent experiments were car-
22 ried out on an epi-fluorescence microscope as described above further equipped with a cage
23 incubator (Okolab, Shanghai, China). Cells were grown at 25 °C overnight on antibody-
24 patterned surfaces and treated with SIINFEKL peptide as indicated. For induction of K^b FHC

1 association, cells were mounted on pre-warmed microscopy stage, and imaging of the
2 GFP signal was started when the medium reached 37 °C.

3 **Fluorescence contrast quantitation.** Contrast analysis was performed as described previ-
4 ously (Lanzerstorfer et al., 2014) In short, initial imaging recording was supported by the
5 Nikon NIS Elements software. Images were exported as TIFF frames and fluorescence con-
6 trast analysis was performed with the Spotty framework (Borgmann et al., 2012). The fluo-
7 rescence contrast $\langle c \rangle$ was calculated as

$$\langle c \rangle = \frac{(F^+ - F^-)}{(F^+ - F_{bg})}$$

8 , where F^+ is the intensity of the inner pixels of the pattern, F^- the intensity of the sur-
9 rounding pixels of the micropattern, and F_{bg} the intensity of the global background.

10

11 **Single molecule microscopy**

12 **Imaging.** Cells were transferred 48 h post transfection onto glass coverslips coated with a
13 poly-L-lysine-graft-(polyethylene glycol) copolymer functionalized with RGD tripeptide to
14 minimize non-specific binding of fluorescent nanobodies (You et al., 2014). Cells imaged in
15 presence of SL8 peptide (sequence SIINFEKL) were pre-incubated with 1 μ M of SL8 pep-
16 tide 12 h before imaging. Single-molecule imaging experiments were conducted by total in-
17 ternal reflection fluorescence (TIRF) microscopy with an inverted microscope (Olympus
18 IX83) equipped with a motorized 4-Line TIR illumination condenser (Olympus) and a back-
19 illuminated electron multiplying (EM) CCD camera (iXon Ultra 897, Andor Technology). A
20 100 \times magnification objective with a numerical aperture of 1.45 (UPLAPO 100 \times HR, NA 1.5,
21 Olympus) together with a 1.6 \times magnification changer was used for TIR illumination of the
22 sample. Imaging was conducted with or without 1 μ M of fresh SL8 peptide. The sample was

1 preincubated with 10 µg/mL of Brefeldin A (BFA) for 15 min in order to inhibit protein
2 transport of GFP-K^b/β₂m heterodimers to the plasma membrane. All experiments were car-
3 ried out at 37 °C in medium without phenol red supplemented with an oxygen scavenger and
4 a redox-active photoprotectant to minimize photobleaching (Vogelsang et al., 2008) and pen-
5 icillin and streptomycin (PAA). For cell surface labeling of GFP-K^b, a 1:1 mixture of anti-
6 GFP nanobodies (2 nM each) site-specifically conjugated with ATTO 643 and ATTO Rho11
7 (Wilmes et al., 2020b), respectively, were added to the medium, thus ensuring >90 % binding
8 given the 0.3 nM binding affinity (Kirchhofer et al., 2010). After incubation for at least
9 5 min, image acquisition was started with the labeled nanobodies kept in the bulk solution
10 during the whole experiment in order to ensure high equilibrium binding. Dimerization of the
11 positive control was induced by applying 0.3 nM of a tandem nanobody crosslinker
12 (LaG16V2) binding to an orthogonal epitope (Fridy et al., 2014). For single molecule co-
13 localization and co-tracking experiments, orange (ATTO Rho11) and red (ATTO 643) emit-
14 ting fluorophores were simultaneously excited by illumination with a 561 nm laser (MPB
15 Communications) and a 642 nm laser (MPB Communications). Fluorescence was detected
16 with a spectral image splitter (QuadView QV2, Photometrics) with a dichroic beam splitter
17 (Chroma) combined with the bandpass filter 600/37 (BrightLine HC) for detection of
18 ATTO Rho11 and 685/40 (Brightline HC) for detection of ATTO 643 dividing each emission
19 channel into 256 × 256 pixels. Image stacks of 150 frames were recorded for each cell at a
20 time resolution of 32 ms/frame. Diffusion constants were determined by mean square dis-
21 placement analysis within a time window of 320 ms (10 frames).

22 **Single molecule analysis.** MHC homodimerization was quantified based on sequential co-
23 localization and co-tracking analysis using self-written Matlab code “SlimFAST “ as de-
24 scribed in detail previously (Roder et al., 2014; Wilmes et al., 2015b). After aligning ATTO
25 643 and ATTO Rho11 channels with sub-pixel precision through spatial transformation based

1 on a calibration measurement with multicolor fluorescent beads (TetraSpeck microspheres
2 0.1 μ m, Invitrogen), individual molecules detected in both spectral channels of the same
3 frame within a distance threshold of 100 nm were considered to be co-localized. For SMCT
4 analysis, the multiple-target tracing (MTT) algorithm was applied to this dataset of co-
5 localized molecules to reconstruct co-locomotion trajectories (co-trajectories) from the identi-
6 fied population of co-localizations. For the co-tracking analysis, only co-trajectories with
7 a minimum of 10 consecutive steps (320 ms) were considered. This cut-off was determined
8 based on systematic analysis of a negative control experiment with non-interacting model
9 transmembrane proteins (Wilmes et al., 2020b) in order to minimize background from ran-
10 dom co-localization. The relative fraction of co-tracked molecules was determined with re-
11 spect to the absolute number of trajectories from both channels and corrected for homodimers
12 stochastically double-labeled with the same fluorophore species as follows:

$$AB^* = \frac{AB}{2 \times \left[\left(\frac{A}{A+B} \right) \times \left(\frac{B}{A+B} \right) \right]}$$

$$rel. co-locomotion = \frac{2 \times AB^*}{(A+B)}$$

13 where A, B, AB and AB* are the numbers of trajectories observed for ATTO Rho11,
14 ATTO 643, co-trajectories and corrected co-trajectories, respectively.
15 For **Figures 3F and 3G**, the relative fraction of co-localized mobile and immobile molecules
16 was determined with respect to the absolute number of mobile or immobile molecules from
17 both channels and corrected for homodimers stochastically double-labeled with the same
18 fluorophore species as follows:

$$AB^* = \frac{AB/A + AB/B}{2}$$

$$rel.\ fraction = \frac{AB^*}{2 \times \left[\left(\frac{A}{A+B} \right) \times \left(\frac{B}{A+B} \right) \right]}$$

1 where A, B, AB and AB* are the numbers of molecules part of a trajectory observed for

2 ATTO Rho11, ATTO 643, co-localized molecules and corrected co-localized molecules, re-
3 spectively.

4 Immobile molecules were classified by their appearance within a radius described by the lo-
5 calization precision and molecular observation probability.

6

7 **Statistics and statistical analysis.** For **Figure 3D-H**, each data point represents the analy-
8 sis from one cell, with ≥ 14 cells measured per experiment and many trajectories analyzed per
9 cell (**3D**, 238-2513; **3E**, 238-2513; **3F**, 314-2732; **3G**, 41-354 tracked immobile particles and
10 362-3141 mobile particles; **3H**, 2-301 co-trajectories). Statistical significances were calculat-
11 ed by two-sample Kolmogorov-Smirnov test, Kruskal-Wallis test with multiple comparisons,
12 unpaired *t* test and two-way ANOVA with multiple comparisons as indicated in the figure
13 legends, using version Prism 8.4.0 for MacOS (GraphPad, San Diego, USA). Box plots were
14 used for visualization and indicate the data distribution of second and third quartile (box),
15 median (line), mean (square) and data range (whiskers).

16

17 **Native mass spectrometry**

18 In advance of native MS measurements, a small amount (<1%) of covalent dimers of the
19 α_3 domain, which had formed as side product during refolding, were removed by size exclu-
20 sion chromatography on Superdex 75 10/300 GL (Cytiva). Amicon Ultra 0.5 mL centrifugal
21 filter units (molecular weight cut-off 3 kDa; Merck Millipore) were used at 14,000 x g and
22 4 °C to exchange purified protein samples to 150 mM ammonium acetate (99.99 %; Sigma-

1 Aldrich), pH 7.2. The final concentration of the α_3 domain monomer was 5 μM , 10 μM or
2 20 μM . Native MS analysis was implemented on a Q-Tof II mass spectrometer in positive
3 electrospray ionization mode. The instrument was modified to enable high mass experiments
4 (Waters and MS Vision, (van den Heuvel et al., 2006)). Sample ions were introduced into the
5 vacuum using homemade capillaries via a nano-electrospray ionization source in positive ion
6 mode (source pressure: 10 mbar). Borosilicate glass tubes (inner diameter: 0.68 mm, outer
7 diameter: 1.2 mm; World Precision Instruments) were pulled into closed capillaries in a two-
8 step program using a squared box filament (2.5 mm \times 2.5 mm) within a micropipette puller
9 (P-1000, Sutter Instruments). The capillaries were then gold-coated using a sputter coater
10 (5.0×10^{-2} mbar, 30.0 mA, 100 s, 3 runs to vacuum limit 3.0×10^{-2} mbar argon, distance of
11 plate holder: 5 cm; CCU-010, safematic). Capillaries were opened directly on the sample
12 cone of the mass spectrometer. In regular MS mode, spectra were recorded at a capillary
13 voltage of 1.45 kV and a cone voltage of 100 V to 150 V. Protein species with quaternary
14 structure were assigned by MS/MS analysis. These experiments were carried out using argon
15 as collision gas (1.2×10^{-2} mbar). The acceleration voltage ranged from 10 V to 100 V.
16 Comparability of results was ensured as MS quadrupole profiles and pusher settings were
17 kept constant in all measurements. A spectrum of cesium iodide (25 g/L) was recorded on the
18 same day of the particular measurement to calibrate the data.

19 All spectra were evaluated regarding experimental mass (MassLynx V4.1, Waters) and ar-
20 ea under the curve (AUC; UniDec (Marty et al., 2015)) of the detected mass species. The
21 values of the shown averaged masses and AUC of the different species as well as the corre-
22 sponding standard deviation result from at least three independent measurements. Exact ex-
23 perimental masses are presented in **Supplementary Figure S4A**.

24

1 **Molecular model of the K^b heavy chain dimer**

2 The crystal structure of K^b in complex with a chicken ovalbumin epitope (PDB 3p9m)
3 served as template to generate a model of the heavy chain dimer. Using the Pymol program
4 (DeLano, 2002), it was possible to superimpose a copy of the 3p9m heavy chain on the β_2m
5 subunit of a second 3p9m structure (FHC dimer). The superposition involved only the match-
6 ing of the α_3 domain backbone of the K^b molecule (residues 181-277) onto the β_2m subunit
7 resulting in a small root-mean-square deviation (RMSD) of 1.25 Å. Very little steric overlap
8 of the superimposed α_3 domain with the second heavy chain was detected. This minimal
9 overlap of the α_1/α_2 domain of the superimposed heavy chain was removed by adjusting
10 backbone dihedral angles of residues 179-181 in the linker between α_1/α_2 domain and the α_3
11 domain. The initial structural model was energy-minimized to remove any residual steric
12 overlap and was prepared for molecular dynamics (MD) simulations using the Amber18
13 package (Case et al., 2018).

14

15 **Molecular docking**

16 For comparison of FHC homodimers and K^b HC/ β_2m heterodimers, MD simulations were
17 performed starting from the coordinates of the K^b structure in PDB 3p9m. Proteins were
18 solvated in octahedral boxes including explicit sodium and chloride ions (0.15 M) and explic-
19 it TIP3P water molecules keeping a minimum distance of 10 Å between protein atoms and
20 box boundaries (Jorgensen et al., 1983). The parm14SB force field was used for the proteins
21 and peptides (Maier et al., 2015). The simulation systems were again energy minimized
22 (5000 steps) after solvation followed by heating up to 300 K in steps of 100 K with position
23 restraints on all heavy atoms of the proteins. Subsequently, positional restraints were gradual-
24 ly removed from an initial 25 kcal·mol⁻¹·Å⁻² to 0.5 kcal·mol⁻¹·Å⁻² within 0.5 ns followed by a

1 1 ns unrestrained equilibration at 300 K. All production simulations were performed at a
2 temperature of 300 K and a pressure of 1 bar. The hydrogen mass repartition option of Amber
3 was used to allow a time step of 4 fs (Hopkins et al., 2015). Unrestrained production simula-
4 tions for up to 400 ns were performed. The interface packing was analyzed by calculation of
5 the buried surface area using the Shrake method, (Shrake and Rupley, 1973); analysis of root-
6 mean-square deviations (RMSD) was performed using the cpptraj module of the Amber18
7 package.

8

9 **High-speed atomic force measurements for antibody density estimation**

10 We employed high-speed atomic force microscopy (HS-AFM), capable of resolving indi-
11 vidual antibodies on surfaces (Preiner et al., 2014; Strasser et al., 2020) to estimate the anti-
12 body surface density in our pattern elements. Antibody micropatterns were prepared as de-
13 scribed above. Antibody solution (10 μ g/mL) was finally incubated for 15 – 1200 s, followed
14 by washing and imaging in PBS. HS-AFM (RIBM, Japan) was operated in tapping mode at
15 room temperature with free amplitudes of 1.5-2.5 nm and an amplitude set point of larger
16 than 90%. Silicon nitride cantilevers (USC-F1.2-k0.15, Nanoworld AG, Neuchâtel, Switzer-
17 land) with nominal spring constants of 0.1-0.15 N/m, resonance frequencies of \sim 500 kHz,
18 and a quality factor of \sim 2 in liquids were used.

19 Since the antibody coverage after 20 min incubation was too high to discriminate and
20 count individual molecules, the images of the shortest incubation time (15 s) were used and
21 thus lowest coverage and largest distance between individual molecules to estimate the area
22 coverage per antibody (neglecting potential tip convolution effects). A height threshold of 2.7
23 nm above the streptavidin layer was applied for detection of particle density and mean area
24 per particle (\sim 190 nm²), which were then used to convert the total area above the threshold in

1 the other images (30 s – 20 min) into a surface density. The resulting surface density Γ of
2 antibodies as a function of incubation time is reasonably described by a mono-exponential
3 function as typical for a pseudo-first order reaction (Artelsmair et al., 2008), i.e.

$$\Gamma(t) = A \left(1 - e^{-t/\tau}\right)$$

4 with $A = 7646 \pm 1828 \text{ IgGs}/\mu\text{m}^2$ (and $\tau = 77 \pm 43 \text{ s}$). Image analysis was performed using
5 threshold algorithms in Gwyddion (Nečas and Klapetek, 2012).

6

7 Acknowledgements

8 We thank the donors of reagents as mentioned in the Materials, Venkat Raman
9 Ramnarayan for comments on the manuscript, Christian P. Richter for support with
10 SMT/SMCT evaluation, Ankur Saikia and Christian Guenther for performing protein chro-
11 matography, the iBiOs staff for technical support with single molecule microscopy, the SPC
12 facility at EMBL Hamburg for technical support, and Uschi Wellbrock for excellent technical
13 assistance.

14

15 Funding

16 Deutsche Forschungsgemeinschaft (DFG SP583/7-2), Bundesministerium für Bildung und
17 Forschung (BMBF, 031A153A); Tönjes Vagt Foundation (XXXII), iNEXT-Discovery
18 (11911), Jacobs University (all to SSp); Deutsche Forschungsgemeinschaft (SFB 944,
19 projects P8 and Z, Facility iBiOs, PI 405/14-1) to JP. PL and JW acknowledge funding from
20 the province of Upper Austria as a part of the FH Upper Austria Center of Excellence for
21 Technological Innovation in Medicine (TIMed Center) and the Christian Doppler For-
22 schungsgesellschaft (Josef Ressel Center for Phylogenetic Drug Research). CU acknowledges

1 funding from the Leibniz Association through SAW-2014-HPI-4 grant. The Heinrich-Pette-
2 Institute, Leibniz Institute for Experimental Virology is supported by the Free and Hanseatic
3 City Hamburg and the German Federal Ministry of Health.

4

5 **Author Contributions**

6 The experimental work was performed as follows: CD, Fig. 1CDEG; ZH, Fig. 1F; PL, Fig.
7 2, 4AB, S1, S2, S4B; SL, Fig. 3, S3, supplementary movies; ARH, Fig. 4CD and S4B; JDK,
8 Fig. 4E-G, S4A; MZ, Fig. 5, S5; AK and JPr, Figure S1AB. MGA, CU, JW and JPi super-
9 vised and interpreted experiments. MZ performed all MD simulations (Fig. 5, 5S1). SSp con-
10 ceived the work, supervised and coordinated experiments, and wrote the manuscript in coop-
11 eration with JPi and PL and assistance by NL with input from all authors. Funding was ac-
12 quired by CU, JPi, JW, MGA, MZ, PL, and SSp.

13

14 **Competing Interests:**

15 The authors declare that no competing interests exist.

16

1 References

2 Allen RL, O'Callaghan CA, McMichael AJ, Bowness P. 1999. Cutting edge: HLA-B27 can
3 form a novel beta 2-microglobulin-free heavy chain homodimer structure. *J Immunol
4 Baltim Md* **162**:5045–5048.

5 Anjanappa R, Garcia-Alai M, Kopicki J-D, Lockhauserbäumer J, Aboelmagd M, Hinrichs J,
6 Nemtanu IM, Utrecht C, Zacharias M, Springer S, Meijers R. 2020. Structures of
7 peptide-free and partially loaded MHC class I molecules reveal mechanisms of pep-
8 tide selection. *Nat Commun* **11**:1314. doi:10.1038/s41467-020-14862-4

9 Antoniou AN, Giuliano DB, Lenart I, Burn G, Powis SJ. 2011. The oxidative folding and
10 misfolding of human leukocyte antigen-b27. *Antioxid Redox Signal* **15**:669–684.
11 doi:10.1089/ars.2010.3692

12 Armony G, Heck AJR, Wu W. 2021. Extracellular crosslinking mass spectrometry reveals
13 HLA class I – HLA class II interactions on the cell surface. *Mol Immunol* **136**:16–25.
14 doi:10.1016/j.molimm.2021.05.010

15 Arosa FA, Esgalhado AJ, Reste-Ferreira D, Cardoso EM. 2021. Open MHC Class I Con-
16 formers: A Look through the Looking Glass. *Int J Mol Sci* **22**:9738.
17 doi:10.3390/ijms22189738

18 Arosa FA, Santos SG, Powis SJ. 2007. Open conformers: the hidden face of MHC-I mole-
19 cules. *Trends Immunol* **28**:115–123. doi:10.1016/j.it.2007.01.002

20 Artelsmair H, Kienberger F, Tinazli A, Schlapak R, Zhu R, Preiner J, Wruss J, Kastner M,
21 Saucedo-Zeni N, Hoelzl M, Rankl C, Baumgartner W, Howorka S, Blaas D, Gruber
22 HJ, Tampé R, Hinterdorfer P. 2008. Atomic force microscopy-derived nanoscale chip
23 for the detection of human pathogenic viruses. *Small Wein Bergstr Ger* **4**:847–854.
24 doi:10.1002/smll.200700691

25 Bahadur RP, Zacharias M. 2008. The interface of protein-protein complexes: Analysis of
26 contacts and prediction of interactions. *Cell Mol Life Sci* **65**:1059–1072.
27 doi:10.1007/s00018-007-7451-x

28 Baia D, Pou J, Jones D, Mandelboim O, Trowsdale J, Muntasell A, Lopez-Botet M. 2016.
29 Interaction of the LILRB1 inhibitory receptor with HLA class Ia dimers. *Eur J Immu-
30 nol* **46**:1681–90. doi:10.1002/eji.201546149

31 Baía D, Pou J, Jones D, Mandelboim O, Trowsdale J, Muntasell A, López-Botet M. 2016.
32 Interaction of the LILRB1 inhibitory receptor with HLA class Ia dimers. *Eur J Immu-
33 nol* **46**:1681–1690. doi:10.1002/eji.201546149

34 Barnstable C. 1978. Production of monoclonal antibodies to group A erythrocytes, HLA and
35 other human cell surface antigens-new tools for genetic analysis. *Cell* **14**:9–20.
36 doi:10.1016/0092-8674(78)90296-9

37 Blumenthal D, Edidin M, Gheber LA. 2016. Trafficking of MHC molecules to the cell sur-
38 face creates dynamic protein patches. *J Cell Sci* **129**:3342–3350.
39 doi:10.1242/jcs.187112

40 Bodnar A, Bacso Z, Jenei A, Jovin TM, Edidin M, Damjanovich S, Matko J. 2003. Class I
41 HLA oligomerization at the surface of B cells is controlled by exogenous beta(2)-
42 microglobulin: implications in activation of cytotoxic T lymphocytes. *Int Immunol*
43 **15**:331–9.

1 Bondar A, Jang W, Sviridova E, Lambert NA. 2020. Components of the Gs signaling cascade
2 exhibit distinct changes in mobility and membrane domain localization upon $\beta 2$ -
3 adrenergic receptor activation. *Traffic Cph Den* **21**:324–332. doi:10.1111/tra.12724

4 Borgmann DM, Weghuber J, Schaller S, Jacak J, Winkler SM. 2012. Identification of pat-
5 terns in microscopy images of biological samples using evolution strategies.

6 Campbell EC, Antoniou AN, Powis SJ. 2012. The multi-faceted nature of HLA class I dimer
7 molecules. *Immunology* **136**:380–384. doi:10.1111/j.1365-2567.2012.03593.x

8 Capps GG, Robinson BE, Lewis KD, Zúñiga MC. 1993. In vivo dimeric association of class I
9 MHC heavy chains. Possible relationship to class I MHC heavy chain-beta 2-
10 microglobulin dissociation. *J Immunol* **151**:159–169.

11 Case DA, Ben-Shalom IY, Brozell SR, Cerutti DS, Cheatham TE III, Cruzeiro VWD, Darde
12 TA, Duke RE, Ghoreishi D, Gilson MK, Gohlke H, Goetz AW, Greene D, Harris R,
13 Homeyer N, Izadi S, Kovalenko A, Kurtzman T, Lee TS, LeGrand S, Li P, Lin C, Liu
14 J, Luchko T, Luo R, Mermelstein DJ, Merz KM, Miao Y, Monard G, Nguyen C,
15 Nguyen H, Omelyan I, Onufriev A, Pan F, Qi R, Roe DR, Roitberg A, Sagui C,
16 Schott-Verdugo S, Shen J, Simmerling CL, Smith J, Salomon-Ferrer R, Swails J,
17 Walker RC, Wang J, Wei H, Wolf RM, Wu X, Xiao L, York DM, Kollman PA. 2018.
18 Amber18. San Fransisco: University of California.

19 Chakrabarti A, Matko J, Rahman NA, Barisas BG, Edidin M. 1992. Self-association of class
20 I major histocompatibility complex molecules in liposome and cell surface mem-
21 branes. *Biochemistry* **31**:7182–9.

22 Chen B, Li J, He C, Li D, Tong W, Zou Y, Xu W. 2017. Role of HLA-B27 in the pathogene-
23 sis of ankylosing spondylitis. *Mol Med Rep* **15**:1943–1951.
24 doi:10.3892/mmr.2017.6248

25 Comber JD, Philip R. 2014. MHC class I antigen presentation and implications for develop-
26 ing a new generation of therapeutic vaccines. *Ther Adv Vaccines* **2**:77–89.
27 doi:10.1177/2051013614525375

28 Dangoria NS, DeLay ML, Kingsbury DJ, Mear JP, Uchanska-Ziegler B, Ziegler A, Colbert
29 RA. 2002. HLA-B27 Misfolding Is Associated with Aberrant Intermolecular Disul-
30 fide Bond Formation (Dimerization) in the Endoplasmic Reticulum. *J Biol Chem*
31 **277**:23459–23468. doi:10.1074/jbc.M110336200

32 Day PM, Esquivel F, Lukszo J, Bennink JR, Yewdell JW. 1995. Effect of TAP on the genera-
33 tion and intracellular trafficking of peptide-receptive major histocompatibility com-
34 plex class I molecules. *Immunity* **2**:137–147. doi:10.1016/S1074-7613(95)80014-X

35 DeLano WL. 2002. Pymol: An open-source molecular graphics tool. *CCP4 Newslett Protein*
36 *Crystallogr* 82–92.

37 Dirscherl C, Hein Z, Ramnarayan VR, Jacob-Dolan C, Springer S. 2018. A two-hybrid anti-
38 body micropattern assay reveals specific in cis interactions of MHC I heavy chains at
39 the cell surface. *eLife* **7**:e34150. doi:10.7554/eLife.34150

40 Dirscherl C, Palankar R, Delcea M, Kolesnikova TA, Springer S. 2017. Specific Capture of
41 Peptide-Receptive Major Histocompatibility Complex Class I Molecules by Antibody
42 Micropatterns Allows for a Novel Peptide-Binding Assay in Live Cells. *Small*
43 **13**:1602974. doi:10.1002/smll.201602974

44 Dulberger CL, McMurtrey CP, Hölzemer A, Neu KE, Liu V, Steinbach AM, Garcia-Beltran
45 WF, Sulak M, Jabri B, Lynch VJ, Altfeld M, Hildebrand WH, Adams EJ. 2017. Hu-
46 man Leukocyte Antigen F Presents Peptides and Regulates Immunity through Interac-

1 tions with NK Cell Receptors. *Immunity* **46**:1018-1029.e7.
2 doi:10.1016/j.jimmuni.2017.06.002

3 Edidin M, Achilles S, Zeff R, Wei T. 1997. Probing the stability of class I major histocom-
4 patibility complex (MHC) molecules on the surface of human cells. *Immunogenetics*
5 **46**:41–45. doi:10.1007/s002510050240

6 Elliott T, Cerundolo V, Elvin J, Townsend A. 1991. Peptide-induced conformational change
7 of the class I heavy chain. *Nature* **351**:402–406. doi:10.1038/351402a0

8 Fassett MS, Davis DM, Valter MM, Cohen GB, Strominger JL. 2001. Signaling at the inhibi-
9 tory natural killer cell immune synapse regulates lipid raft polarization but not class I
10 MHC clustering. *Proc Natl Acad Sci U S A* **98**:14547–14552.
11 doi:10.1073/pnas.211563598

12 Ferez M, Castro M, Alarcon B, van Santen HM. 2014. Cognate peptide-MHC complexes are
13 expressed as tightly apposed nanoclusters in virus-infected cells to allow TCR
14 crosslinking. *J Immunol* **192**:52–8. doi:10.4049/jimmunol.1301224

15 Fooksman DR, Grönvall GK, Tang Q, Edidin M. 2006. Clustering Class I MHC Modulates
16 Sensitivity of T Cell Recognition. *J Immunol* **176**:6673–6680.
17 doi:10.4049/jimmunol.176.11.6673

18 Fridy PC, Li Y, Keegan S, Thompson MK, Nudelman I, Scheid JF, Oeffinger M, Nus-
19 senzweig MC, Fenyö D, Chait BT, Rout MP. 2014. A robust pipeline for rapid pro-
20 duction of versatile nanobody repertoires. *Nat Methods* **11**:1253–1260.
21 doi:10.1038/nmeth.3170

22 Gakamsky DM, Bjorkman PJ, Pecht I. 1996. Peptide Interaction with a Class I Major Histo-
23 compatibility Complex-Encoded Molecule: Allosteric Control of the Ternary Com-
24 plex Stability [†]. *Biochemistry* **35**:14841–14848. doi:10.1021/bi961707u

25 Gamin Y, Lopez-Esparza R, Reffay M, Sierecki E, Gov NS, Genest M, Hodges RS, Urbach
26 W. 2006. Lateral mobility of proteins in liquid membranes revisited. *Proc Natl Acad
27 Sci U S A* **103**:2098–2102. doi:10.1073/pnas.0511026103

28 Garstka M, Borchert B, Al-Balushi M, Praveen P, Kühl N, Majoul I, Duden R, Springer S.
29 2007. Peptide-receptive Major Histocompatibility Complex Class I Molecules Cycle
30 between Endoplasmic Reticulum and *cis* -Golgi in Wild-type Lymphocytes. *J Biol
31 Chem* **282**:30680–30690. doi:10.1074/jbc.M701721200

32 Geng J, Altman JD, Krishnakumar S, Raghavan M. 2018. Empty conformers of HLA-B pref-
33 erentially bind CD8 and regulate CD8+ T cell function. *eLife* **7**:e36341.
34 doi:10.7554/eLife.36341

35 Goodridge JP, Lee N, Burian A, Pyo C-W, Tykodi SS, Warren EH, Yee C, Riddell SR, Ger-
36 aghty DE. 2013. HLA-F and MHC-I Open Conformers Cooperate in a MHC-I Anti-
37 gen Cross-Presentation Pathway. *J Immunol* **191**:1567–1577.
38 doi:10.4049/jimmunol.1300080

39 Graham FL, van der Eb AJ. 1973. A new technique for the assay of infectivity of human ade-
40 novirus 5 DNA. *Virology* **52**:456–467. doi:10.1016/0042-6822(73)90341-3

41 Hein Z, Uchtenhagen H, Abualrous ET, Saini SK, Janssen L, Van Hateren A, Wiek C,
42 Hanenberg H, Momburg F, Achour A, Elliott T, Springer S, Boulanger D. 2014. Pep-
43 tide-independent stabilization of MHC class I molecules breaches cellular quality
44 control. *J Cell Sci* **127**:2885–2897. doi:10.1242/jcs.145334

45 Ho CCM, Chhabra A, Starkl P, Schnorr P-J, Wilmes S, Moraga I, Kwon H-S, Gaudenzio N,
46 Sibilano R, Wehrman TS, Gakovic M, Sockolosky JT, Tiffany MR, Ring AM, Piehler

1 J, Weissman IL, Galli SJ, Shizuru JA, Garcia KC. 2017. Decoupling the Functional
2 Pleiotropy of Stem Cell Factor by Tuning c-Kit Signaling. *Cell* **168**:1041-1052.e18.
3 doi:10.1016/j.cell.2017.02.011

4 Hopkins CW, Le Grand S, Walker RC, Roitberg AE. 2015. Long-Time-Step Molecular Dy-
5 namics through Hydrogen Mass Repartitioning. *J Chem Theory Comput* **11**:1864–
6 1874. doi:10.1021/ct5010406

7 Ibach J, Radon Y, Gelléri M, Sonntag MH, Brunsved L, Bastiaens PIH, Verveer PJ. 2015.
8 Single Particle Tracking Reveals that EGFR Signaling Activity Is Amplified in
9 Clathrin-Coated Pits. *PLoS One* **10**:e0143162. doi:10.1371/journal.pone.0143162

10 Jorgensen WL, Chandrasekhar J, Madura JD, Impey RW, Klein ML. 1983. Comparison of
11 simple potential functions for simulating liquid water. *J Chem Phys* **79**:926–935.
12 doi:10.1063/1.445869

13 Kaufman J. 2018. Generalists and Specialists: A New View of How MHC Class I Molecules
14 Fight Infectious Pathogens. *Trends Immunol* **39**:367–379.
15 doi:10.1016/j.it.2018.01.001

16 Kirchhofer A, Helma J, Schmidthals K, Frauer C, Cui S, Karcher A, Pellis M, Muyldermans
17 S, Casas-Delucchi CS, Cardoso MC, Leonhardt H, Hopfner K-P, Rothbauer U. 2010.
18 Modulation of protein properties in living cells using nanobodies. *Nat Struct Mol Biol*
19 **17**:133–138. doi:10.1038/nsmb.1727

20 Lanzerstorfer P, Borgmann D, Schütz G, Winkler SM, Höglinger O, Weghuber J. 2014.
21 Quantification and kinetic analysis of Grb2-EGFR interaction on micro-patterned sur-
22 faces for the characterization of EGFR-modulating substances. *PLoS One* **9**:e92151.
23 doi:10.1371/journal.pone.0092151

24 Lanzerstorfer P, Müller U, Gordiyenko K, Weghuber J, Niemeyer CM. 2020. Highly Modu-
25 lar Protein Micropatterning Sheds Light on the Role of Clathrin-Mediated Endocytosis
26 for the Quantitative Analysis of Protein-Protein Interactions in Live Cells. *Bio-
27 molecules* **10**:540. doi:10.3390/biom10040540

28 Lin W-C, Iversen L, Tu H-L, Rhodes C, Christensen SM, Iwig JS, Hansen SD, Huang WYC,
29 Groves JT. 2014. H-Ras forms dimers on membrane surfaces via a protein-protein in-
30 terface. *Proc Natl Acad Sci U S A* **111**:2996–3001. doi:10.1073/pnas.1321155111

31 Ljunggren H-G, Stam NJ, Öhlén C, Neefjes JJ, Höglund P, Heemels M-T, Bastin J,
32 Schumacher TNM, Townsend A, Kärre K, Ploegh HL. 1990. Empty MHC class I
33 molecules come out in the cold. *Nature* **346**:476–480. doi:10.1038/346476a0

34 Low-Nam ST, Lidke KA, Cutler PJ, Roovers RC, van Bergen en Henegouwen PMP, Wilson
35 BS, Lidke DS. 2011. ErbB1 dimerization is promoted by domain co-confinement and
36 stabilized by ligand binding. *Nat Struct Mol Biol* **18**:1244–1249.
37 doi:10.1038/nsmb.2135

38 Lu X, Gibbs JS, Hickman HD, David A, Dolan BP, Jin Y, Kranz DM, Bennink JR, Yewdell
39 JW, Varma R. 2012. Endogenous viral antigen processing generates peptide-specific
40 MHC class I cell-surface clusters. *Proc Natl Acad Sci U S A* **109**:15407–15412.
41 doi:10.1073/pnas.1208696109

42 Mahmutefendic H, Blagojevic G, Tomas MI, Kucic N, Lucin P. 2011. Segregation of open
43 Major Histocompatibility Class I conformers at the plasma membrane and during en-
44 dosomal trafficking reveals conformation-based sorting in the endosomal system. *Int
45 J Biochem Cell Biol* **43**:504–515. doi:10.1016/j.biocel.2010.12.002

1 Maier JA, Martinez C, Kasavajhala K, Wickstrom L, Hauser KE, Simmerling C. 2015.
2 ff14SB: Improving the Accuracy of Protein Side Chain and Backbone Parameters
3 from ff99SB. *J Chem Theory Comput* **11**:3696–3713. doi:10.1021/acs.jctc.5b00255

4 Makhadiyeva D, Lam L, Moatari M, Vallance J, Zheng Y, Campbell EC, Powis SJ. 2012.
5 MHC class I dimer formation by alteration of the cellular redox environment and in-
6 duction of apoptosis: Redox control of MHC class I dimer formation. *Immunology*
7 **135**:133–139. doi:10.1111/j.1365-2567.2011.03518.x

8 Marty MT, Baldwin AJ, Marklund EG, Hochberg GKA, Benesch JLP, Robinson CV. 2015.
9 Bayesian Deconvolution of Mass and Ion Mobility Spectra: From Binary Interactions
10 to Polydisperse Ensembles. *Anal Chem* **87**:4370–4376.
11 doi:10.1021/acs.analchem.5b00140

12 Matko J, Bushkin Y, Wei T, Edidin M. 1994. Clustering of class I HLA molecules on the
13 surfaces of activated and transformed human cells. *J Immunol* **152**:3353–60.

14 Montealegre Sebastián, Venugopalan V, Fritzsche S, Kulicke C, Hein Z, Springer S. 2015.
15 Dissociation of β_2 microglobulin determines the surface quality control of major
16 histocompatibility complex class I molecules. *FASEB J* **29**:2780–2788.
17 doi:10.1096/fj.14-268094

18 Montealegre S., Venugopalan V, Fritzsche S, Kulicke C, Hein Z, Springer S. 2015. Dissocia-
19 tion of beta2-microglobulin determines the surface quality control of major histocom-
20 patibility complex class I molecules. *Faseb J* **29**:2780–8. doi:10.1096/fj.14-268094

21 Moraga I, Wernig G, Wilmes S, Gryshkova V, Richter CP, Hong W-J, Sinha R, Guo F, Fabi-
22 onar H, Wehrman TS, Krutzik P, Demharter S, Plo I, Weissman IL, Minary P, Majeti
23 R, Constantinescu SN, Piehler J, Garcia KC. 2015. Tuning cytokine receptor signal-
24 ing by re-orienting dimer geometry with surrogate ligands. *Cell* **160**:1196–1208.
25 doi:10.1016/j.cell.2015.02.011

26 Mylvaganam SM, Grinstein S, Freeman SA. 2018. Picket-fences in the plasma membrane:
27 functions in immune cells and phagocytosis. *Semin Immunopathol* **40**:605–615.
28 doi:10.1007/s00281-018-0705-x

29 Nečas D, Klapetek P. 2012. Gwyddion: an open-source software for SPM data analysis. *Open
30 Phys* **10**. doi:10.2478/s11534-011-0096-2

31 Niman HL, Houghten RA, Walker LE, Reisfeld RA, Wilson IA, Hogle JM, Lerner RA. 1983.
32 Generation of protein-reactive antibodies by short peptides is an event of high fre-
33 quency: implications for the structural basis of immune recognition. *Proc Natl Acad
34 Sci* **80**:4949–4953. doi:10.1073/pnas.80.16.4949

35 Ortiz-Navarrete V, Hammerling GJ. 1991. Surface appearance and instability of empty H-2
36 class I molecules under physiological conditions. *Proc Natl Acad Sci* **88**:3594–3597.
37 doi:10.1073/pnas.88.9.3594

38 Preiner J, Kodera N, Tang J, Ebner A, Brameshuber M, Blaas D, Gelbmann N, Gruber HJ,
39 Ando T, Hinterdorfer P. 2014. IgGs are made for walking on bacterial and viral sur-
40 faces. *Nat Commun* **5**:4394. doi:10.1038/ncomms5394

41 Reinhardt U, Lotze J, Zernia S, Mörl K, Beck-Sickinger AG, Seitz O. 2014. Peptide-
42 Templatet Acyl Transfer: A Chemical Method for the Labeling of Membrane Pro-
43 teins on Live Cells. *Angew Chem Int Ed* **53**:10237–10241.
44 doi:10.1002/anie.201403214

45 Richter D, Moraga I, Winkelmann H, Birkholz O, Wilmes S, Schulte M, Kraich M,
46 Kenneweg H, Beutel O, Selenschik P, Paterok D, Gavutis M, Schmidt T, Garcia KC,

1 Müller TD, Piehler J. 2017. Ligand-induced type II interleukin-4 receptor dimers are
2 sustained by rapid re-association within plasma membrane microcompartments. *Nat*
3 *Commun* **8**:15976. doi:10.1038/ncomms15976

4 Roder F, Wilmes S, Richter CP, Piehler J. 2014. Rapid Transfer of Transmembrane Proteins
5 for Single Molecule Dimerization Assays in Polymer-Supported Membranes. *ACS*
6 *Chem Biol* **9**:2479–2484. doi:10.1021/cb5005806

7 Schell TD. 2002. The assembly of functional beta2-microglobulin-free MHC class I mole-
8 cules that interact with peptides and CD8+ T lymphocytes. *Int Immunol* **14**:775–782.
9 doi:10.1093/intimm/dxf041

10 Schwarzenbacher M, Kaltenbrunner M, Brameshuber M, Hesch C, Paster W, Weghuber J,
11 Heise B, Sonnleitner A, Stockinger H, Schutz GJ. 2008. Micropatterning for quantita-
12 tive analysis of protein-protein interactions in living cells. *Nat Methods* **5**:1053–60.
13 doi:10.1038/nmeth.1268

14 Sevcik E, Brameshuber M, Folser M, Weghuber J, Honigmann A, Schutz GJ. 2015. GPI-
15 anchored proteins do not reside in ordered domains in the live cell plasma membrane.
16 *Nat Commun* **6**:6969. doi:10.1038/ncomms7969

17 Shrake A, Rupley JA. 1973. Environment and exposure to solvent of protein atoms. Ly-
18 sozyme and insulin. *J Mol Biol* **79**:351–371. doi:10.1016/0022-2836(73)90011-9

19 Spack E, Edidin M. 1986. The class I MHC antigens of erythrocytes: a serologic and bio-
20 chemical study. *J Immunol Baltim Md 1950* **136**:2943–2952.

21 Sprague B, McNally J. 2005. FRAP analysis of binding: proper and fitting. *Trends Cell Biol*
22 **15**:84–91. doi:10.1016/j.tcb.2004.12.001

23 Strasser J, de Jong RN, Beurskens FJ, Schuurman J, Parren PW, Hinterdorfer P, Preiner J.
24 2020. Weak Fragment Crystallizable (Fc) Domain Interactions Drive the Dynamic
25 Assembly of IgG Oligomers upon Antigen Recognition. *ACS Nano* **14**:2739–2750.
26 doi:10.1021/acsnano.9b08347

27 Townsend A, Bodmer H. 1989. Antigen recognition by class I -restricted cytotoxic T lym-
28 phocytes. *Annu Rev Immunol* 601–24.

29 Townsend A, Elliott T, Cerundolo V, Foster L, Barber B, Tse A. 1990. Assembly of MHC
30 class I molecules analyzed in vitro. *Cell* **62**:285–295. doi:10.1016/0092-
31 8674(90)90366-M

32 Townsend A, Öhlén C, Bastin J, Ljunggren H-G, Foster L, Kärre K. 1989. Association of
33 class I major histocompatibility heavy and light chains induced by viral peptides. *Nature*
34 **340**:443–448. doi:10.1038/340443a0

35 Triantafilou K, Triantafilou M, Wilson KM, Fernandez N. 2000. Human major histocompati-
36 bility molecules have the intrinsic ability to form homotypic associations. *Hum*
37 *Immunol* **61**:585–598. doi:10.1016/S0198-8859(00)00112-9

38 Vámosi G, Friedländer-Brock E, Ibrahim SM, Brock R, Szöllösi J, Vereb G. 2019. EGF Re-
39 ceptor Stalls upon Activation as Evidenced by Complementary Fluorescence Correla-
40 tion Spectroscopy and Fluorescence Recovery after Photobleaching Measurements.
41 *Int J Mol Sci* **20**:E3370. doi:10.3390/ijms20133370

42 van den Heuvel RHH, van Duijn E, Mazon H, Synowsky SA, Lorenzen K, Versluis C,
43 Brouns SJ, Langridge D, van der Oost J, Hoyes J, Heck AJR. 2006. Improving the
44 Performance of a Quadrupole Time-of-Flight Instrument for Macromolecular Mass
45 Spectrometry. *Anal Chem* **78**:7473–7483. doi:10.1021/ac061039a

1 Váradi T, Schneider M, Sevcik E, Kiesenhofer D, Baumgart F, Batta G, Kovács T, Platzer
2 R, Huppa JB, Szöllösi J, Schütz GJ, Brameshuber M, Nagy P. 2019. Homo- and Het-
3 eroassociations Drive Activation of ErbB3. *Biophys J* **117**:1935–1947.
4 doi:10.1016/j.bpj.2019.10.001

5 Vogelsang J, Kasper R, Steinhauer C, Person B, Heilemann M, Sauer M, Tinnefeld P. 2008.
6 A Reducing and Oxidizing System Minimizes Photobleaching and Blinking of Fluor-
7 escent Dyes. *Angew Chem Int Ed* **47**:5465–5469. doi:10.1002/anie.200801518

8 Wilmes S, Beutel O, Li Z, Francois-Newton V, Richter CP, Janning D, Kroll C, Hanhart P,
9 Hötte K, You C, Uzé G, Pellegrini S, Piehler J. 2015a. Receptor dimerization dynam-
10 ics as a regulatory valve for plasticity of type I interferon signaling. *J Cell Biol*
11 **209**:579–593. doi:10.1083/jcb.201412049

12 Wilmes S, Beutel O, Li Z, Francois-Newton V, Richter CP, Janning D, Kroll C, Hanhart P,
13 Hötte K, You C, Uzé G, Pellegrini S, Piehler J. 2015b. Receptor dimerization dynam-
14 ics as a regulatory valve for plasticity of type I interferon signaling. *J Cell Biol*
15 **209**:579–593. doi:10.1083/jcb.201412049

16 Wilmes S, Hafer M, Vuorio J, Tucker JA, Winkelmann H, Löchte S, Stanly TA, Pulgar
17 Prieto KD, Poojari C, Sharma V, Richter CP, Kurre R, Hubbard SR, Garcia KC, Mo-
18 raga I, Vattulainen I, Hitchcock IS, Piehler J. 2020a. Mechanism of homodimeric cy-
19 tokine receptor activation and dysregulation by oncogenic mutations. *Science*
20 **367**:643–652. doi:10.1126/science.aaw3242

21 Wilmes S, Hafer M, Vuorio J, Tucker JA, Winkelmann H, Löchte S, Stanly TA, Pulgar
22 Prieto KD, Poojari C, Sharma V, Richter CP, Kurre R, Hubbard SR, Garcia KC, Mo-
23 raga I, Vattulainen I, Hitchcock IS, Piehler J. 2020b. Mechanism of homodimeric cy-
24 tokine receptor activation and dysregulation by oncogenic mutations. *Science*
25 **367**:643–652. doi:10.1126/science.aaw3242

26 You C, Richter CP, Löchte S, Wilmes S, Piehler J. 2014. Dynamic Submicroscopic Signaling
27 Zones Revealed by Pair Correlation Tracking and Localization Microscopy. *Anal
28 Chem* **86**:8593–8602. doi:10.1021/ac501127r

29

30

31

32

1 **Figure legends**

2 **Figure 1: MHC I HC/HC association requires dissociation of β_2 m but no disulfide
3 bonds.**

4 A, Schematic of MHC class I states at the plasma membrane. Dissociation of peptide from
5 the HC/ β_2 m/peptide trimer results in an 'empty' HC/ β_2 m heterodimer. Dissociation of β_2 m
6 then produces free HCs (FHCs), which can form FHC associations (HC/HC dimer and oli-
7 gomer shown). Other forms such as disulfide-linked dimers are known depending on the
8 allotype (see the text).

9 B, Schematic representation of the two-hybrid antibody micropattern assay. Cells expressing
10 a class I GFP fusion (green) and an N-terminally HA-tagged class I (gray) are seeded onto
11 glass slides that are printed with micrometer-sized patterns of fluorescently labelled anti-HA
12 antibodies. Dissociation of β_2 m generates FHCs of both constructs, which diffuse freely in
13 the plasma membrane and eventually associate with each other to form HC/HC dimers (cen-
14 ter) or oligomers (not shown). The HC/HC associations, which contain both HA-tagged and
15 GFP-fused FHCs, localize in the pattern elements and are visible as pattern-shaped GFP fluo-
16 rescence on the plasma membrane.

17 C, Representative fluorescence micrograph showing one single STF1 cell expressing both
18 HA-tagged and GFP-fused H-2K^b in phase contrast (left), the purple anti-HA antibody pat-
19 tern on the glass slide (middle), and green K^b-GFP colocalizing with the antibody pattern
20 (right). The arrows point to the fluorophore observed in the respective panel and emphasize
21 the plane of the image. Scale bar, 20 μ m.

22 D, Interaction occurs between HA-tagged K^b and D^b-GFP FHCs (37 °C) but not between
23 HC/ β_2 m heterodimers (25 °C). Scale bar, 20 μ m.

24 E, HC/HC interaction does not involve intracellular disulfide bond formation, since the FHCs
25 (37 °C) of HA-K^b and K^b(C332S) GFP, which lacks the cytosolic cysteine, interact in the
26 micropattern assay. Scale bar, 20 μ m.

27 F, B27, but not K^b, forms covalent dimers. HA-K^b (K^b in the label) and HA-B*27:05 (B27)
28 molecules were immunoprecipitated from the lysate of transduced STF1 cells with an anti-
29 HA monoclonal antibody, separated by reducing (+) or nonreducing (-) SDS-PAGE, and
30 monomers (heavy chain) and covalent homodimers as indicated were detected by Western
31 blotting with an anti-HA antiserum. * denotes a background band.

32 G, No interaction of K^b-GFP with F \square pocket-stabilized HA-K^b(Y84C/A139C), a disulfide-
33 stabilized K^b variant with increased β_2 m affinity. Scale bar, 20 μ m.

34

35 **Figure 2: FHCs interact in TAP-proficient cells and in the absence of patterns.**

36 A, Schematic of cell surface interaction between FHCs in TAP2-deficient (left) and TAP2-
37 proficient cells.

38 B, Time course of the interaction between HA-K^b and K^b-GFP in the anti-HA antibody
39 micropattern assay upon temperature shift from 25 °C to 37 °C in TAP2-proficient

1 (STF1/TAP2, right) and TAP2-deficient cells (STF1, left). Representative TIRF microscopy
2 images are shown. 2 μ M of cognate SIINFEKL peptide were added as indicated. Scale bar, 8
3 μ m. Insets show enlarged intensity-adjusted regions within the selected cells.

4 **C**, Quantification of fluorescence contrast from B. Error bars are standard error of the mean
5 (SEM) of >10 cells measured in ≥ 2 independent experiments.

6 **D**, FRAP analysis of K^b cell surface dynamics. Cells expressing K^b constructs as in B were
7 monitored in the absence of patterns (top) or on anti-HA antibody patterns (bottom) with or
8 without SIINFEKL peptide as indicated. Regions in the red circle were bleached, and recov-
9 ery of fluorescence was followed over time. Scale bar, 5 μ m. Insets show the enlarged inten-
10 sity-adjusted region of bleached spot.

11 **E**, Normalized mean fluorescence recovery curves from FRAP experiments, error bars repre-
12 sent SEM of >20 cells for each condition measured in >2 independent experiments.

13 **F**, Diffusion coefficients calculated from E. Significant increase in diffusion coefficients up-
14 on peptide addition, both in the absence and presence of antibody patterns. ****, $p \leq 0.0001$
15 by two-way ANOVA. ns, not significant. Error bars are SEM of >20 cells for each condition
16 measured in ≥ 2 independent experiments.

17 **G**, Immobile fraction of K^b -GFP molecules, i.e. molecules that remain in the bleached area
18 during the time of the experiment. With peptide vs. without peptide ****, $p \leq 0.0001$ and on
19 pattern vs. in the absence of pattern ****, $p \leq 0.0001$ by two-way ANOVA. Error bars are
20 SEM of >20 cells for each condition measured in ≥ 2 independent experiments.

21 **H**, Exchange rates of K^b molecules calculated from fluorescence recovery curves. k_{fast} (left Y
22 axis, hatched bars) is the rate of diffusion of K^b -GFP molecules. k_{slow} (right Y axis, solid-
23 color bars) is the rate of K^b -GFP exchange on (= binding to and dissociation from) HA- K^b .
24 With peptide vs. without peptide ****, $p \leq 0.0001$ on anti-HA pattern by two-way ANOVA.
25 Error bars are SEM of >20 cells for each condition measured in ≥ 2 independent experiments.

26

27 **Figure 3: Single-molecule microscopy shows K^b dimer formation.**

28 **A**, Schematic on the left: analyzing FHC association by single-molecule microscopy. GFP-
29 K^b molecules at the plasma membrane were labeled with two different fluorophores (ATTO
30 Rho11, magenta, and ATTO 643, green) using anti-GFP nanobodies, with one GFP molecule
31 binding one nanobody. Diffusion and interaction of individual molecules was quantified by
32 tracking and co-tracking of individual molecules. Right: Top view of the plasma membrane
33 with diffusing and co-diffusing nanobody-labeled GFP- K^b molecules (corresponding data
34 are shown in **C**).

35 **B**, Formation and dissociation of an individual GFP- K^b dimer detected by co-tracking analy-
36 sis. Co-locomoting molecules are highlighted by a white square. Scale bar, 400 nm.

37 **C**, Single molecule trajectories (green, magenta) and co-trajectories (black) observed for
38 GFP- K^b FHCs (no peptide, top) and HC/ β_2 m/peptide trimers (With peptide, middle). As a
39 control, the same experiment was carried out after crosslinking peptide-loaded K^b with a tan-
40 dem anti-GFP nanobody (With crosslinker, bottom). Scale bar, 2 μ m.

1 **D-H**, statistical analyses by two-sample Kolmogorov-Smirnov test (****, $p \leq 0.0001$; ***, $p \leq 0.001$; **, $p \leq 0.01$). Sample numbers see the methods section.

2 **D**, Fraction of detected co-trajectories out of the total number of observed trajectories for K^b in the absence and in the presence of peptide and crosslinker as indicated.

3 **E**, Diffusion coefficients of K^b molecules determined by single-molecule tracking in the absence and presence of peptide and crosslinker.

4 **F**, The fraction of immobile molecules out of the total GFP- K^b surface molecules determined by single-molecule tracking. SIINFEKL peptide and crosslinker were added as indicated.

5 **G**, Comparison of the fractions of mobile and immobile GFP- K^b molecules that are associated. The fraction of (associated immobile K^b)/(total immobile K^b) is shown vs. the fraction of (associated mobile K^b)/(total mobile K^b).

6 **H**, Quantification of co-trajectory half-life for GFP- K^b as obtained from single molecule co-trajectories with SIINFEKL peptide and crosslinker as indicated; the dissociation rates calculated from the means are 3.1 (no peptide), 17 (peptide, no crosslinker), and 1.3 s^{-1} (with peptide and crosslinker).

16

17 **Figure 4: The $K^b \square_3$ domains form dimers.**

18 **A**, HC/HC association between HA- K^b -RFP and α_3 -GFP. Distance between pattern elements, 2 μm .

19 **B**, HC/HC association between HA- α_3 and α_3 -GFP. Distance between pattern elements, 2 μm .

20 **C**, Size exclusion chromatography of the $K^b \alpha_3$ domain expressed in E.coli and folded in vitro.

21 **D**, Nonreducing SDS-PAGE of the α_3 domain homodimer fraction from C shows absence of disulfide linkage between the monomers. The positive control for disulfide oligomer formation is α_3 inclusion bodies, isolated under oxidizing conditions, where some molecules are linked by disulfide bonds to form covalent oligomers as indicated on the left.

22 **E**, MS/MS analysis of the α_3 domain at 10 μM . The 9+ peak at 2551 m/z corresponding to the α_3 dimer was selected for MS/MS analysis at 10 V, 50 V and 100 V in the collision cell. The dimer (double spheres) easily dissociates in the gas-phase indicating a non-covalent rather low-affinity binding event. At 50 V, no dimer is detectable anymore displaced by monomeric signal (single spheres).

23 **F**, Overall area under the curve (AUC) for the detected α_3 domain dimers. Native mass spectra were recorded using 5 μM , 10 μM or 20 μM α_3 domain at 10 V (dark red) and 25 V (light red), respectively. The AUC was determined over the entire spectrum for the dimeric mass species and is shown as mean ($n=3$) \pm SD. The dimeric fraction is concentration-dependent.

24 **G**, Representative mass spectra (20 μM α_3 domain) show the charge distributions of monomer (single sphere) and dimer (double spheres) at 10 V (dark red) and 25 V (light red) in the collision cell.

1

2 **Figure 5: One hypothetical model of a K^b FHC dimer.**

3 In this hypothetical structure of the extracellular portion of an FHC dimer (**A**), one of several
4 structures predicted by computational molecular docking and molecular dynamics simulation,
5 the α_3 domain of one FHC (orange) binds to another FHC (yellow/purple/lavender) in a man-
6 ner resembling the binding of β_2 m in the crystal structure of peptide-loaded K^b (**B**, PDB
7 3P9L).

8

9 **Tables**

10

11 **Table 1:** Comparison of diffusion coefficients (mean \pm SD in $\mu\text{m}^2/\text{s}$). NA, not applicable.

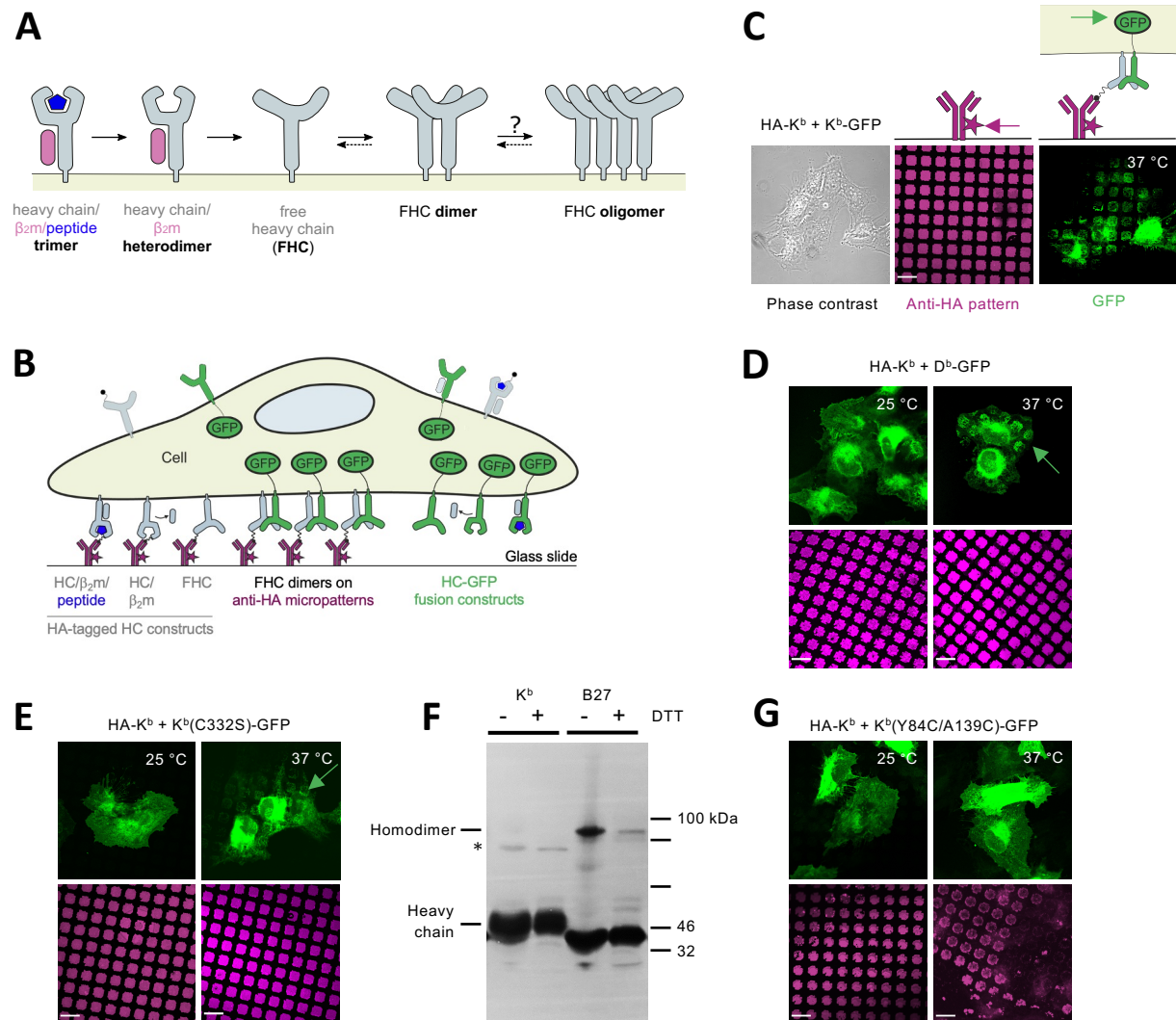
	FRAP	SMT
HC/β_2m/peptide trimers (+peptide)	0.35 ± 0.12	0.35 ± 0.06
FHCs (-peptide)	0.19 ± 0.05	0.25 ± 0.04
FHCs (-peptide)^a	0.19 ± 0.05	0.18 ± 0.10
Dimerized HC/β_2m/peptide trimers (+peptide, + CL)	NA	0.20 ± 0.05
Dimerized HC/β_2m/peptide trimers (+peptide, + CL)^a	NA	0.15 ± 0.04

12

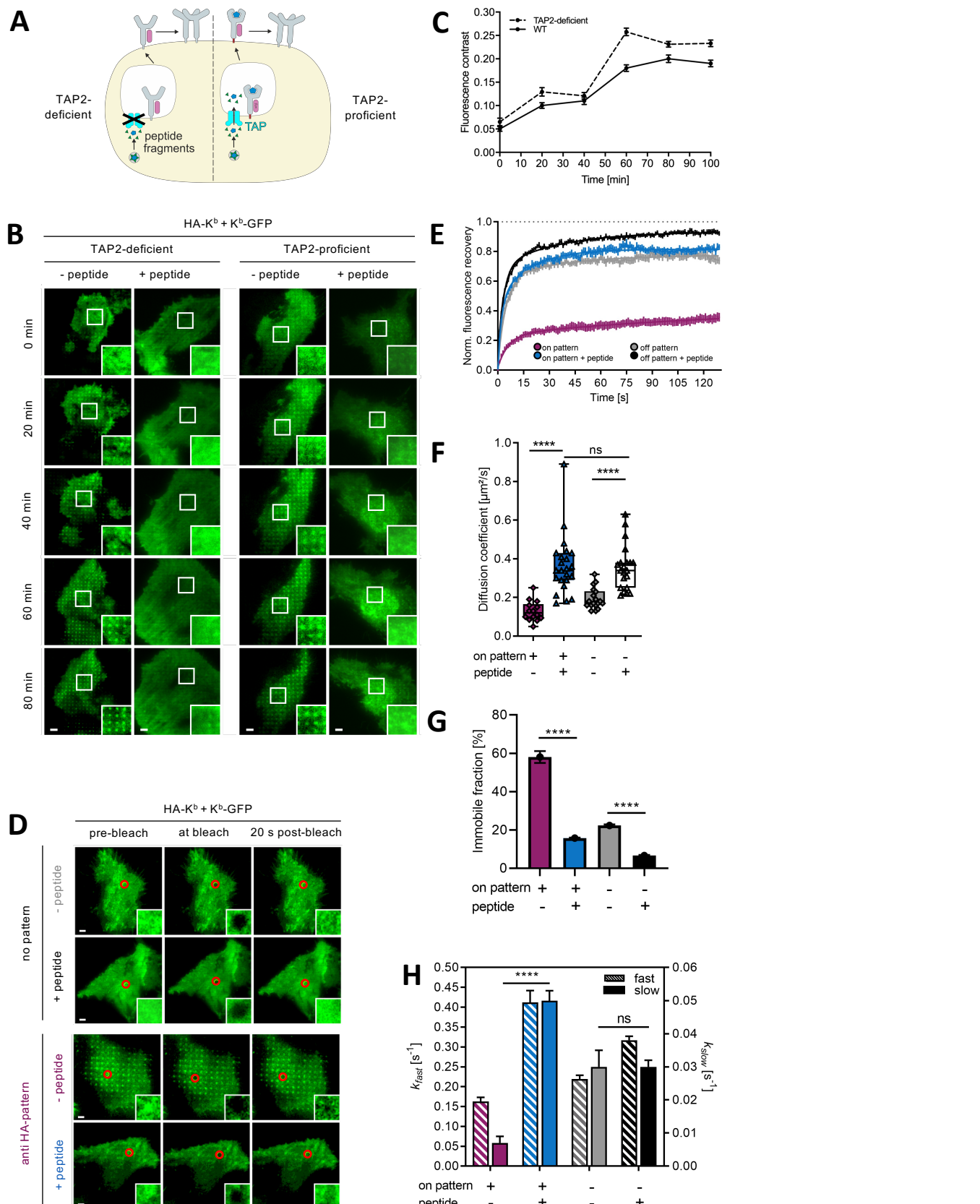
^aonly dimers identified by SMCT

13

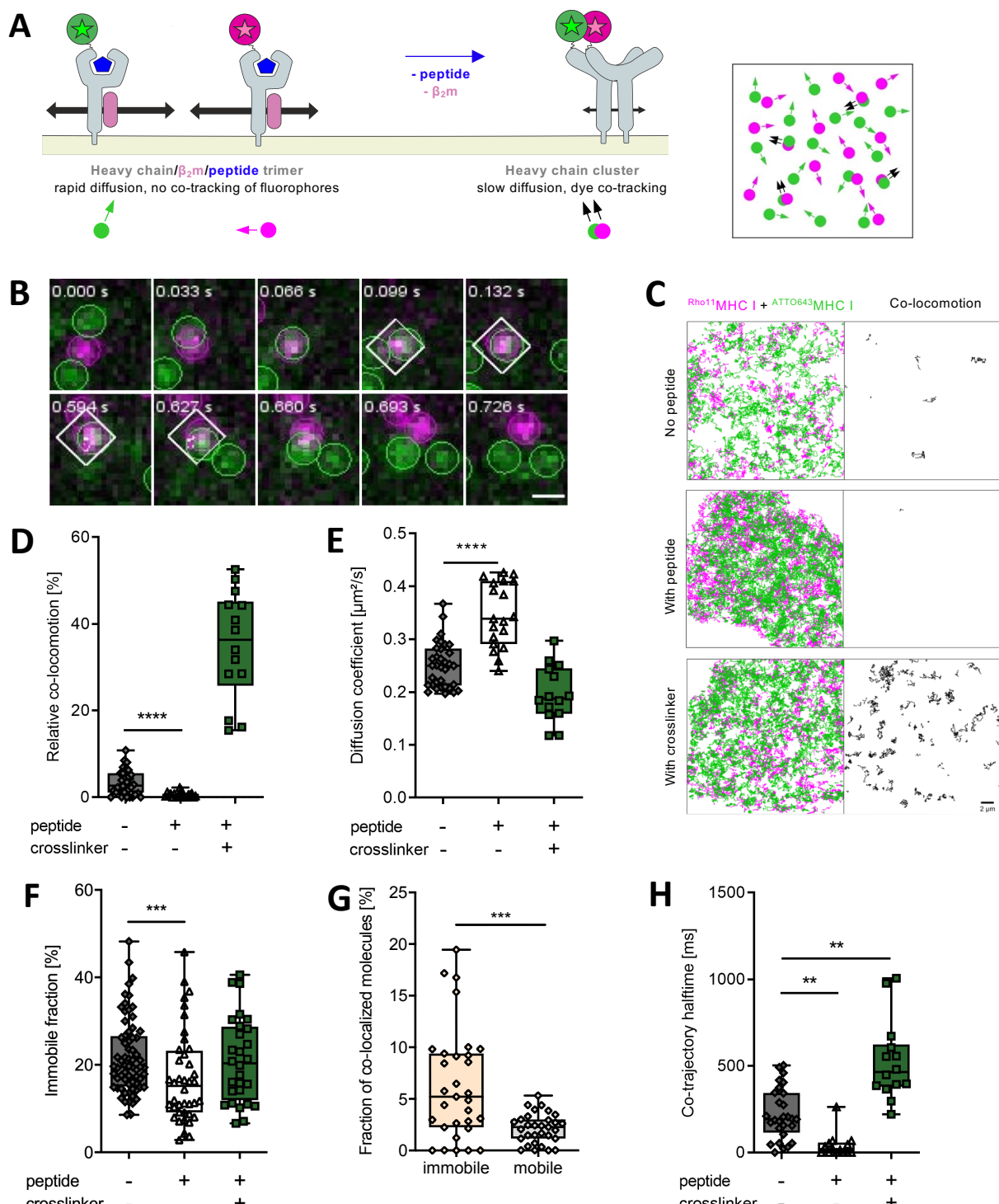
Dirscherl *et al.*, Figure 1



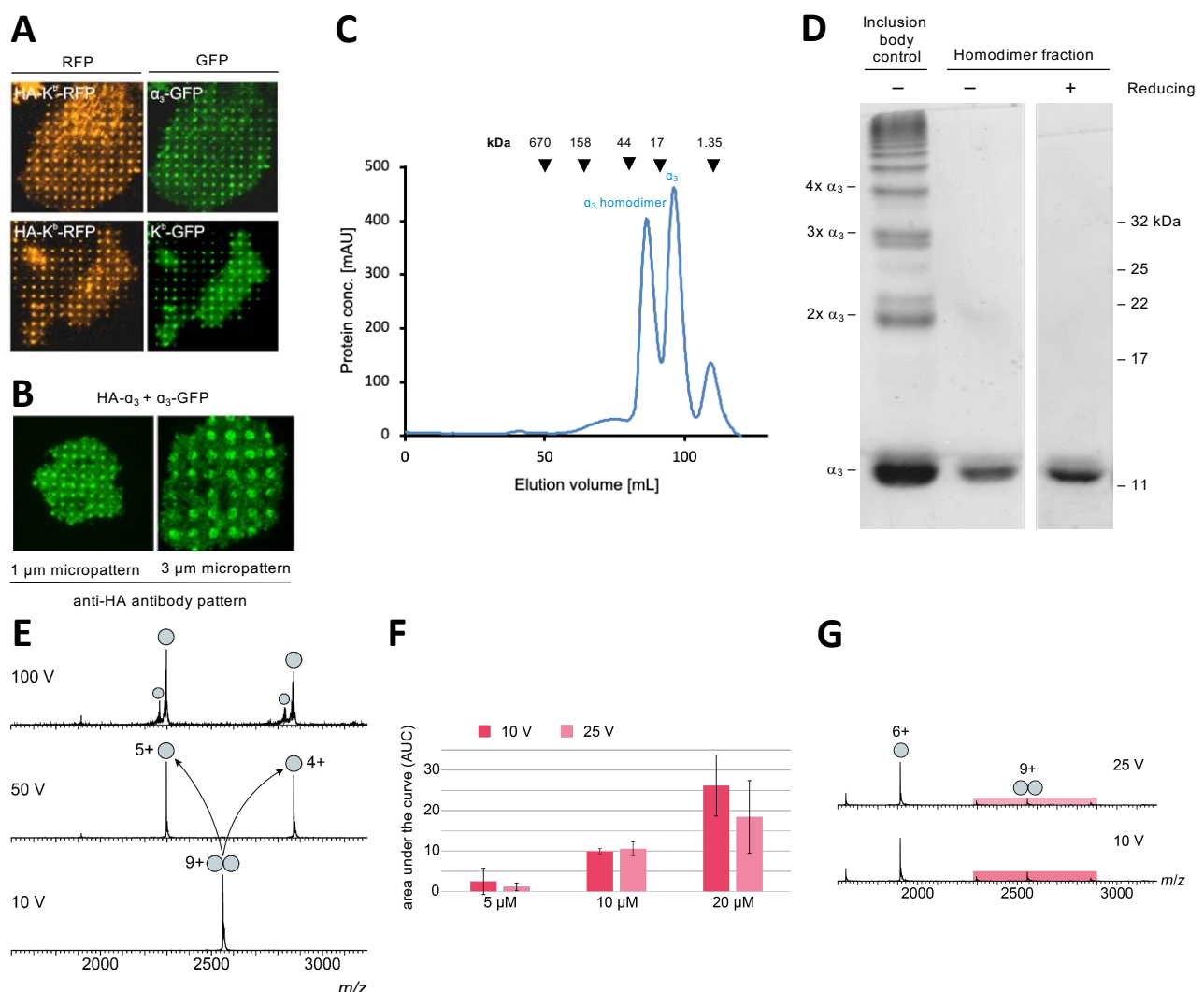
Dirscherl *et al.*, Figure 2



Dirscherl *et al.*, Figure 3



Dirscherl *et al.*, Figure 4



Dirscherl *et al.*, Figure 5

